Argonne NATIONAL LABORATORY

ANL/ESD/13-3

Wind Tunnel Model of the Turner-Fairbank Highway Research Center Aerodynamics Laboratory

TFHRC Project Report

ANL/ESD/13-3

Wind Tunnel Model
of the Turner-Fairbank Highway Research Center Aerodynamics Laboratory

by
S.A. Lottes[1] and C. Bojanowski[1]
[1] Transportation Research and Analysis Computing Center (TRACC)
Energy Systems Division, Argonne National Laboratory

submitted to
Kornel Kerenyi[1] and Harold Bosch[1]
[1] Turner-Fairbank Highway Research Center

May 2013

Table of Contents

List of Figures

List of Tables

1. Introduction and Objectives

The computational fluid dynamics (CFD) and computational structural mechanics (CSM) focus areas at Argonne's Transportation Research and Analysis Computing Center (TRACC) initiated a project to support and compliment the experimental programs at the Turner-Fairbank Highway Research Center (TFHRC) with high performance computing based analysis capabilities in August 2010. The project was established with a new interagency agreement between the Department of Energy and the Department of Transportation to provide collaborative research, development, and benchmarking of advanced three-dimensional computational mechanics analysis methods to the aerodynamics and hydraulics laboratories at TFHRC for a period of five years, beginning in October 2010. The analysis methods employ well benchmarked and supported commercial computational mechanics software. Computational mechanics encompasses the areas of Computational Fluid Dynamics (CFD), Computational Wind Engineering (CWE), Computational Structural Mechanics (CSM), and Computational Multiphysics Mechanics (CMM) applied in Fluid-Structure Interaction (FSI) problems.

This report documents one of the tasks in this project. In this task, a detailed CFD model of the wind tunnel laboratory at TFHRC was built and tested to provide a means to assess the air flow uniformity provided by the tunnel to the test zone and assess room geometry effects. Considerable effort went into the construction and testing of the model and various submodels, such as the screens in the wind tunnel. The model is available for use in further studies.

2. Initial Modeling of the Wind Tunnel Laboratory at TFHRC

A study of the TFHRC wind tunnel using CFD modeling was initiated in the 4th quarter of FY2011. It's goals were to provide TFHRC researchers with the answers to the following questions:

- What is the overall quality of the flow in the testing section of the tunnel?
- What is the influence of the room walls' proximity on the air flow in the room?
- What is the influence of the room setup (including layout of the furniture and the equipment) on the flow quality?

2.1. Wind Tunnel CAD Geometry and Mesh Construction

Pictures of the room and wind tunnel are shown in Figure 2.1 and Figure 2.2. A CAD data file containing the detailed geometry of the wind tunnel was initially provided by TFHRC (see Figure 2.3). It was importable to STAR-CCM+, although the geometry of the fan and fan inlets were overly simplified and required modifications.

Figure 2.1 Laboratory door side of wind tunnel near the largest cross section

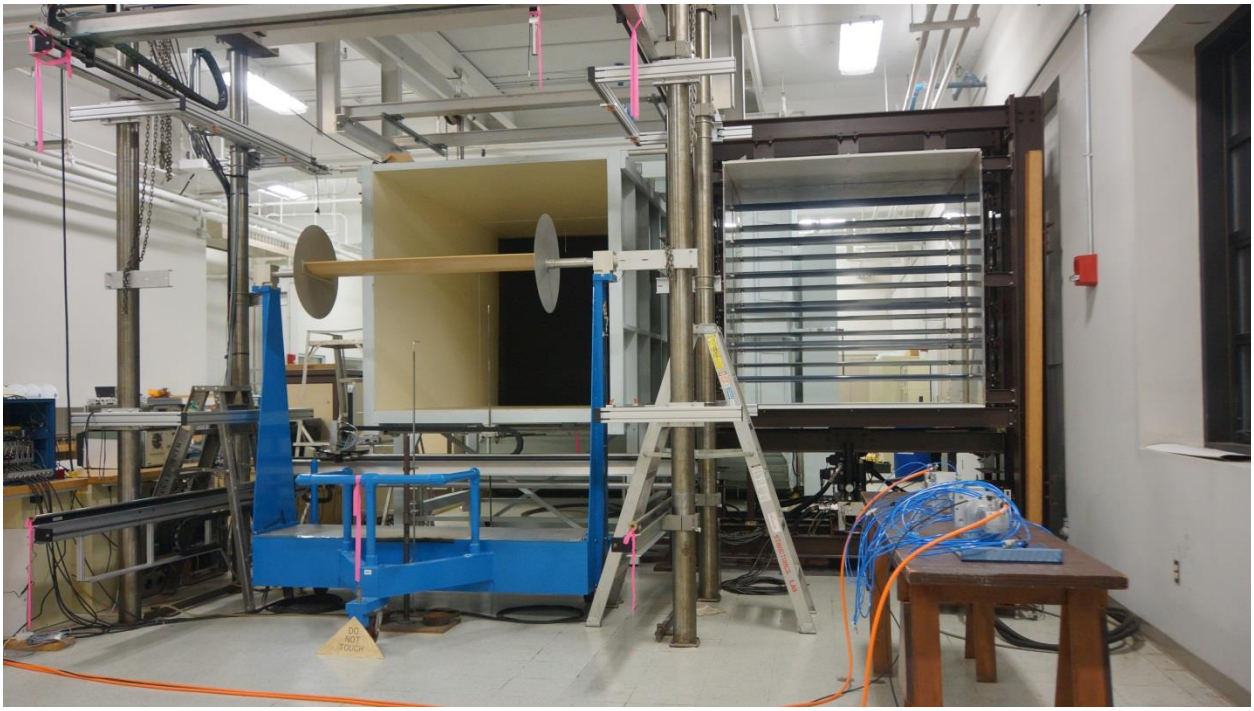

Figure 2.2 Exit of wind tunnel showing test object suspended in the wind tunnel jet region and the turbulence generator out of the wind tunnel on the right.

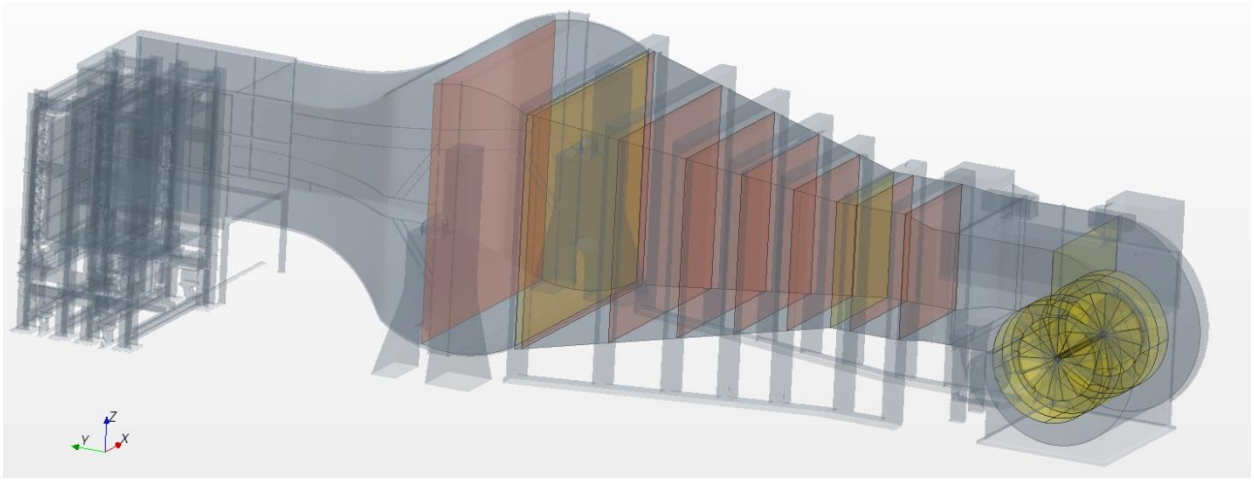

Figure 2.3: CAD model imported to STAR-CCM+

Figure 2.4 and Figure 2.5 show changes that were made to these parts of the model. Although the fan inlets closely resemble the real shape now, the fan geometry is still too simplified and in future may need additional improvements. Nevertheless, for the purpose of this study, it is believed that the actual geometry of the fan and inlets should provide reasonably good results for engineering assessment of the effects of room walls and furniture on wind tunnel air flow.

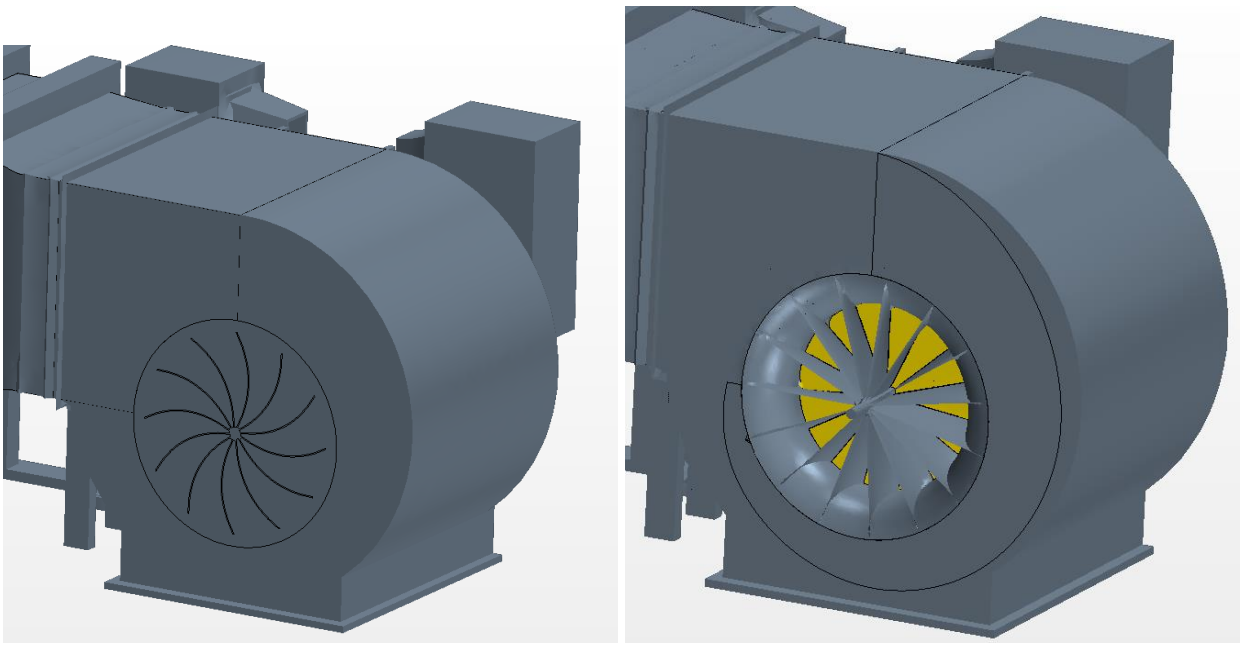

Figure 2.4: Geometry of the fan inlets: initial (left) and updated (right)

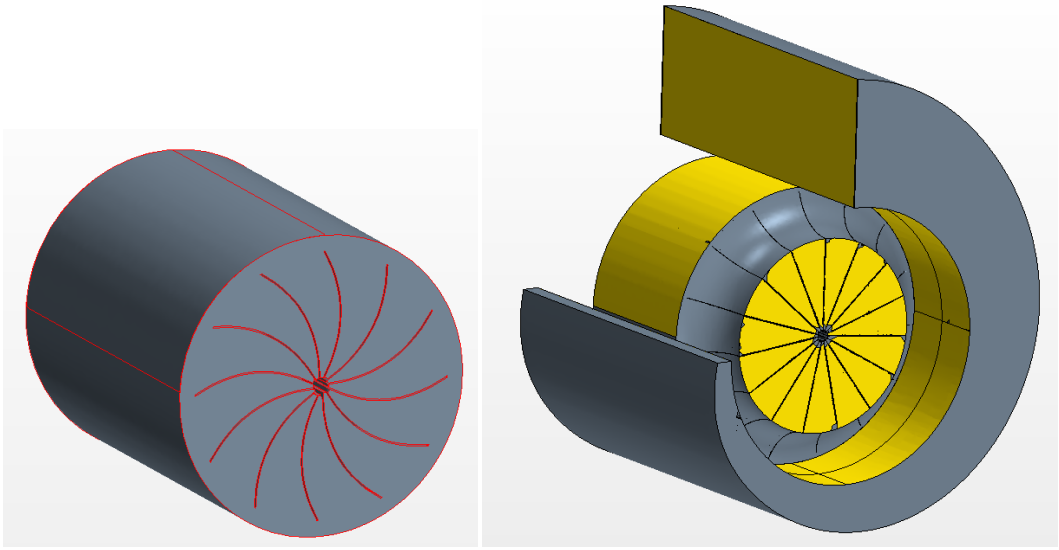

Figure 2.5: Geometry of the fan: initial (left) and updated (right)

The geometry was divided into several regions that have separate meshing settings. Nine regions for the tunnel, two regions for the fan assembly and one for the rest of the model were created. The densest mesh was defined in the fan region due to its geometrical complexity. A fine mesh was needed in order for the surface wrapper to fill the volume entirely. The entire model contained almost 3,500,000 cells. Several cross sections through it showing the mesh are shown in Figure 2.6.

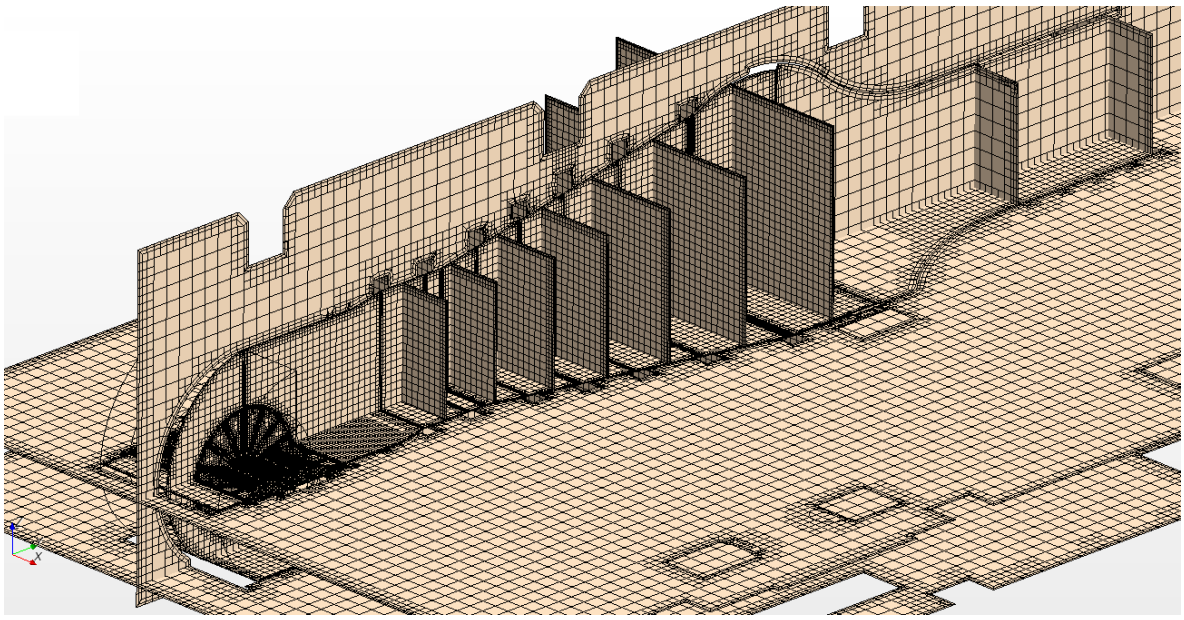

Figure 2.6: cross sections through the model

The interaction between the regions in the model was further defined by interfaces. The interfaces are highlighted in Figure 2.3 by yellow and orange colors. The yellow ones represent continuous in-place interfaces that do not cause any losses in the flow pressure while the orange ones represent porous baffles.

2.2. Porous Baffle Model

The porous baffles were defined at the locations where screens are installed in the real tunnel. The porosity of the screens was determined to be 0.672 based on the specification sheets provided by TFHRC [1]. According to the STAR-CCM+ user guide [2] the pressure drop across a porous baffle can be modeled with the following equation:

$$\Delta p = -\rho(\alpha|v_n| + \beta)v_n \qquad 2.1$$

Where ρ is the density of air and v_n is the normal velocity of air acting on the screen and α and β are parameters that depend on screen geometry and properties.

In [3], this relation is reduced to only the quadratic term with parameter K:

$$\Delta p = -\frac{1}{2}K\rho {v_n}^2 \qquad 2.2$$

Setting parameter β to zero in Equation **2.1** we can now relate α to the K parameter as:

$$K = 2\alpha \qquad 2.3$$

The simplest Borda-Carnot one-dimensional formula for screen pressure-drop coefficient defines K as follows [4]:

$$K = \frac{1-\chi}{\chi^2} \quad 2.4$$

Where χ is the open area ratio (χ = 0.672).

As a first approximation parameters for the porous baffle were assumed constant for each screen as: α = 0.3632 and β = 0. However, it should be noted that this formula may overestimate K for high Re numbers [4]. A more advanced formula by Weighardt defines *K* as [4]:

$$K = 6.5\left[\frac{1-\chi}{\chi^2}\right]\left[\frac{v_n d}{\chi v}\right]^{-0.33} \quad 2.5$$

Where v_n is the air velocity normal to the screens, d is the screen wire diameter and ν is the kinematic viscosity of the air.

Taking the diameter of the screen wire as 0.0075 inch, the kinematic viscosity of air as 15.68e-6 m/s^2 and its constant velocity on all screens to be 20 m/s, this formula yields:

$$K = 0.91\frac{1-\chi}{\chi^2} \quad 2.6$$

This simple calculation shows that the constant K may be substantially overestimated depending on the velocity of the air on the screen. Now that the approximate velocities of the air on the screens are known, a second iteration can be conducted with more accurate values for K calculated from Equation 2.5.

Another important feature of the model was the rotating fan. To introduce the rotation effect on the flow, a rotating reference system was defined with one axis going through the axis of the fan. A constant velocity of 500 rotations per minute was assigned to the system and the fan. This is one operating speed of the fan as per TFHRC specifications.

2.3. First Tests of the Wind Tunnel Model without Furniture in the Room

The first set of simulations model the system without the furniture in the room to determine the characteristics of the flow field in an empty room as a base case. Figure 2.7 shows velocity profiles in the room and the tunnel at a vertical plane through the center of the tunnel. Note that the velocity in the extension of the tunnel and the testing section (just in the front of the tunnel) appears quite uniform. In a horizontal plane about mid-height through the tunnel the flow in the room is asymmetrical (see Figure 2.8). The left side (looking downstream) is blocked by the turbulence generator. In the original model the vanes in the generator were in a closed position. The mass flow through the fan inlet on the left side

was 18.713 kg/s (15.54 m^3/s) and 17.058 kg/s (14.17 m^3/s) on the right side. The right side inlet is obstructed with a pulley plate for turning the fan.

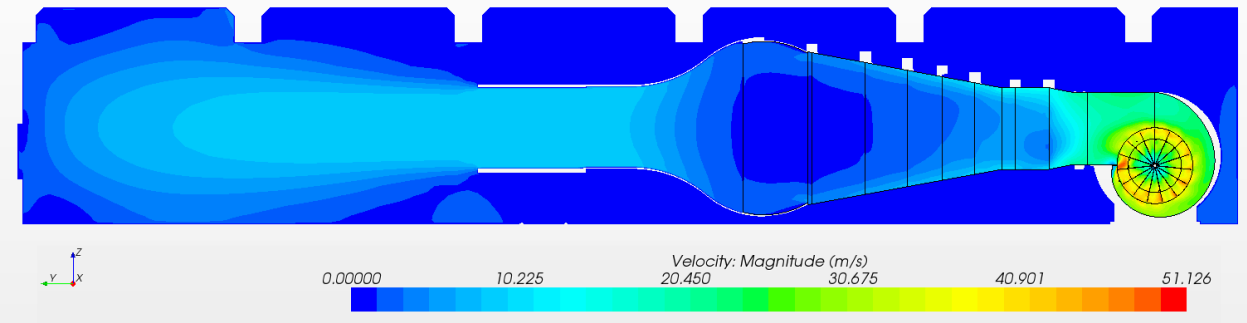

Figure 2.7: Velocity profile in model without the furniture – vertical plane

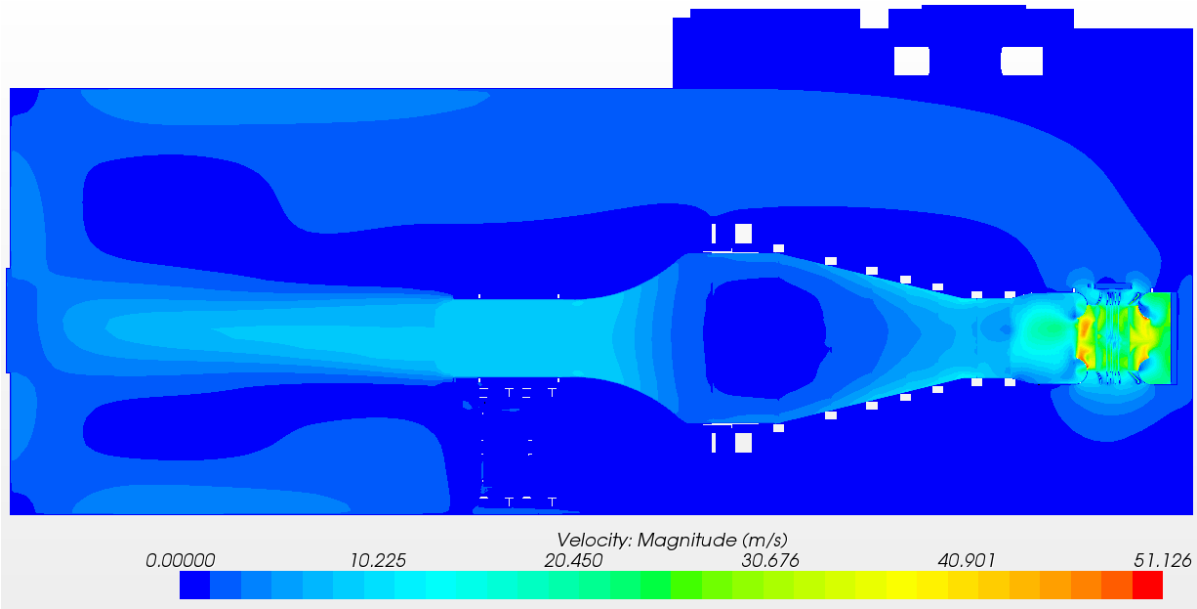

Figure 2.8: Velocity profile in model without the furniture – horizontal plane

Figure 2.9 presents the pressure profile in the wind tunnel. Significant drops of pressure are noted as expected across the screens.

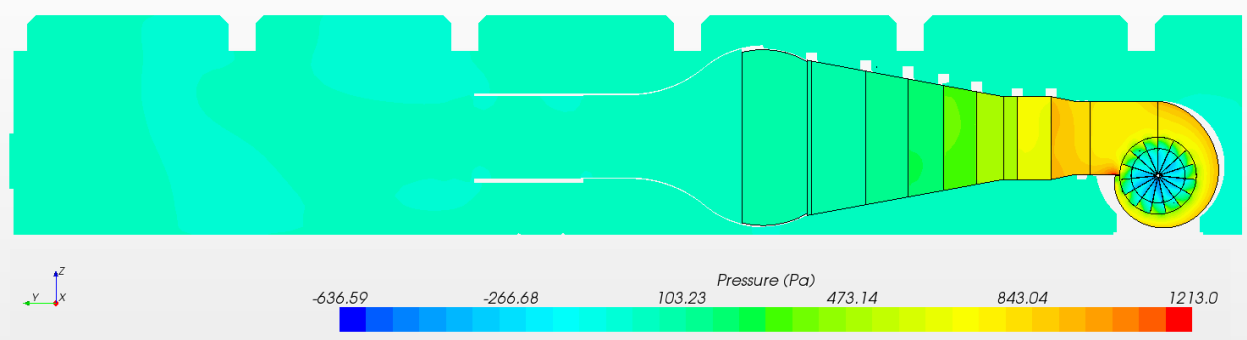

Figure 2.9: Pressure profile in the wind tunnel

To check how the turbulence generator is influencing the flow, the vanes in it were rotated to their neutral position. The generator itself was not moved from its initial position on the left side of the extension part of the tunnel. In this model the mass flow has changed only slightly: from 17.058 kg/s (14.17 m^3/s) to 16.63 kg/s (14.04 m^3/s) on the side blocked with the fan pulley plate and from 18.713 kg/s (15.54 m^3/s) to 19.25 kg/s (16.25 m^3/s) on the open (left) side.

2.4. Tests of Flow through the Tunnel with Screens Removed

In the initial simulations the velocity of the air was higher in the tunnel in the near downstream of the fan near the boundaries of the tunnel. This appears to be counterintuitive at first and additional simulation was performed where the screens – porous baffles – were replaced with the in-place interfaces to eliminate them as the cause of the flow distribution. With no porous baffles, there is no pressure drop across the interfaces at the tunnel sections in the model. This simplified model was supposed to provide more insight into the flow and help identify if any potential errors were produced by the definitions of the porous baffles. Figure 2.10 and Figure 2.11 show the velocity profile obtained from the simulation with this simplified model. Note that for this case the velocity is still highest on the top of the tunnel. This behavior is attributable to the rotating elements of the fan releasing the air at a tangent to the fan's circumference. On the bottom wall of the tunnel the velocity is also high since the air coming off the fan blades is meeting an obstacle. The flow inside of the tunnel and in the testing section is highly non-uniform. This shows the need for the screens inside of the tunnel to produce a near uniform flow in the downstream.

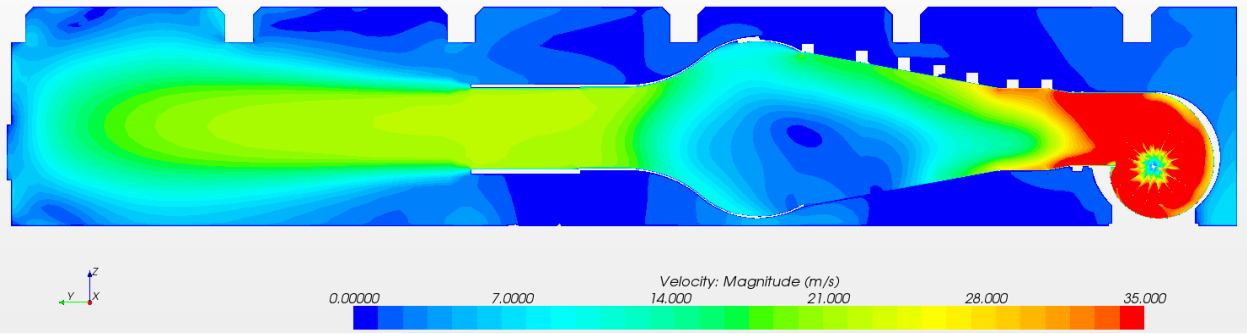

Figure 2.10: Velocity profile in model without the furniture and no screens – vertical plane

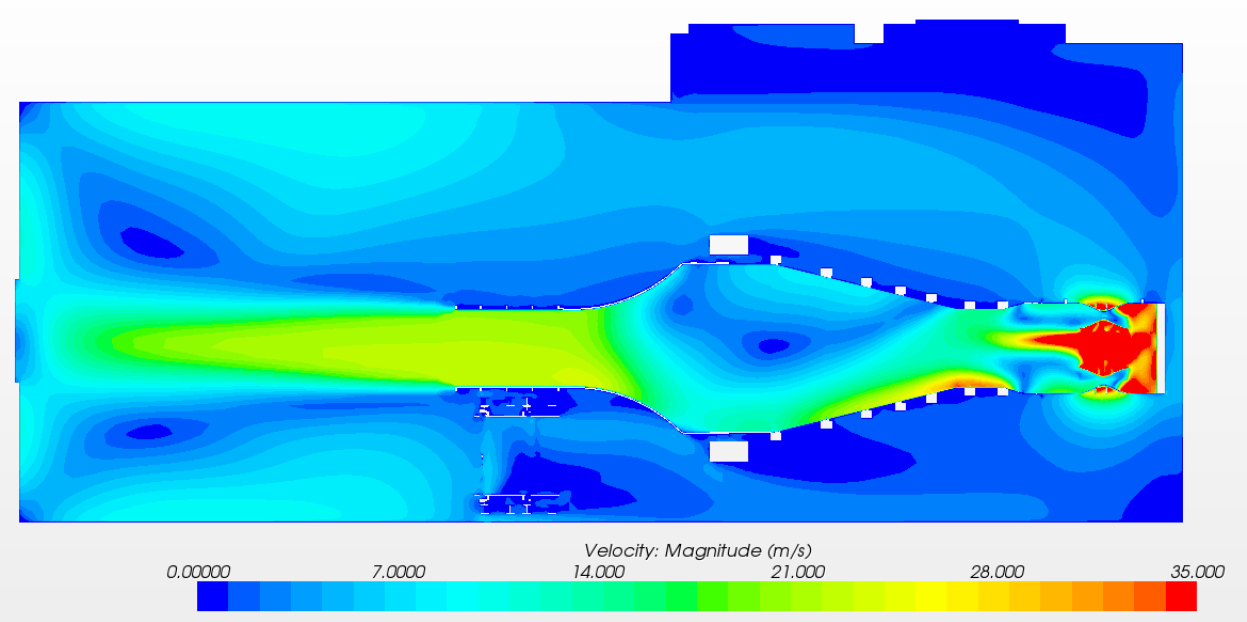

Figure 2.11: Velocity profile in model without the furniture and no screens – horizontal plane

The lack of the screens contributed significantly to the increase of the air mass flow through the fan inlets. The mass flow rate increased to 39.06 kg/s (32.98 m^3/s) and to 47.32 kg/s (39.96 m^3/s) on the right and left sides respectively.

2.5. Test of the Wind Tunnel Model Centered in a large Room

The next test conducted on the model was with a symmetric room where the walls were moved away from the tunnel, 10 meters each. Also the ceiling was raised 5 meters. Additionally the turbulence generator was removed from the model. This test was conducted to see how "ideal" conditions would change the flow pattern. Figure 2.12 shows the horizontal cross section through the model. The velocity profile is more symmetric than in the previous cases. The dark blue spans a velocity range between 0 and a little less than 2 m/s, causing the return flow not to show up in the plot because it is less than 2 m/s.

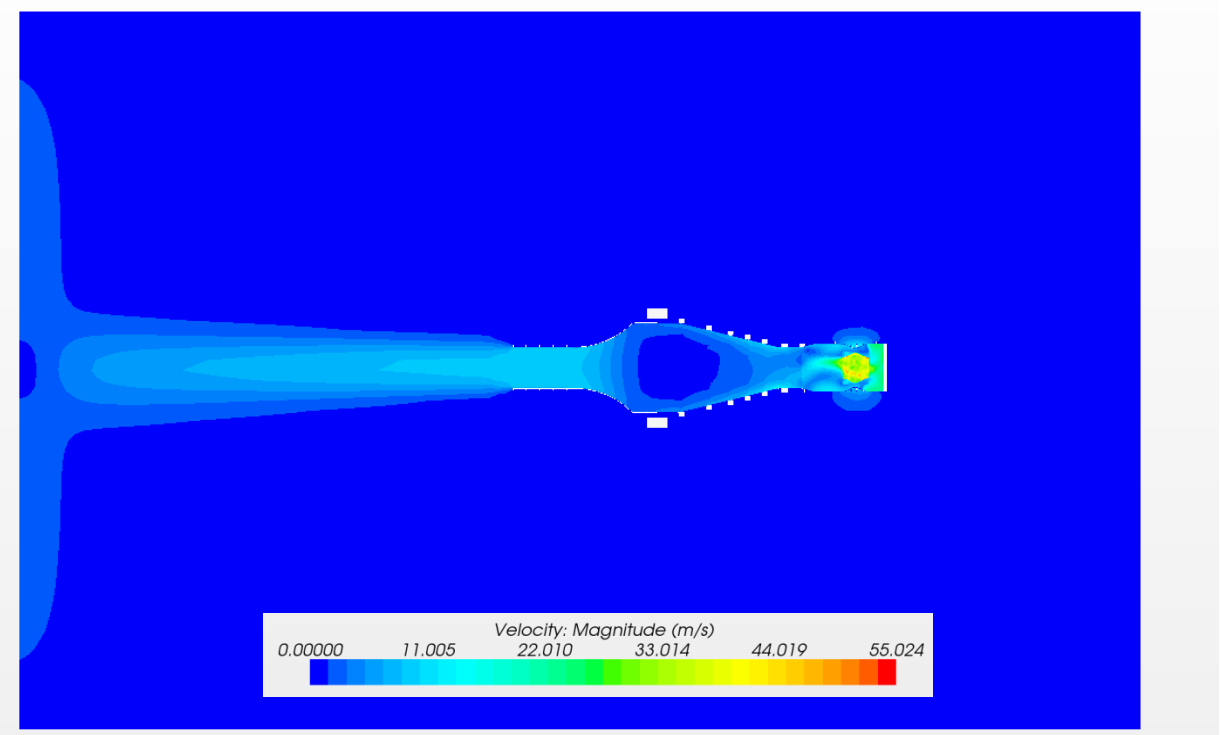

Figure 2.12: Velocity profile in model extended boundaries – horizontal plane

Surprisingly the air mass flow through the fan inlets didn't change much in comparison to the initial models. It has changed from 17.058 kg/s (14.17 m^3/s) to 16.70 kg/s (14.10 m^3/s) on the side blocked with the fan pulley plate (right side) and from 18.713 kg/s (15.54 m^3/s) to 18.87 kg/s (15.94 m^3/s) on the left side.

2.6. Flow Uniformity in Wind Tunnel Sections

In order to quantify the changes in the flow through the tunnel area, a standard deviation and coefficient of variation of the velocity at nine cross sections in the tunnel were calculated. The location of nine cross sections of interest is shown in Figure 2.13. Seven of them were located between the screens and an additional two in the tunnel extension.

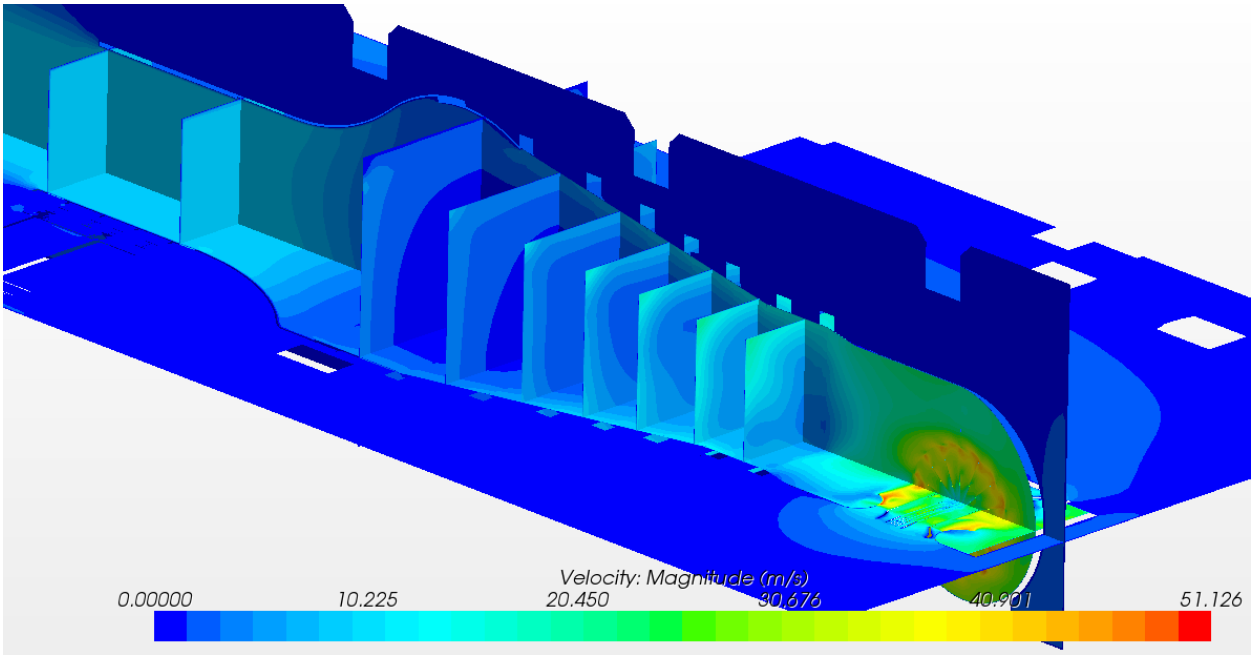

Figure 2.13: Sections of interest in the tunnel

The area averaged standard deviations of the velocity for three models:

- initial, without the furniture, with the turbulence generator vanes closed
- initial, without the furniture, with the turbulence generator vanes in neutral position
- without the furniture with extended boundaries, without the turbulence generator

are plotted in Figure 2.14. It can be noted that a slight difference between the curves can only be noticed at the first two screens. The standard deviation does not take into account the fact that the mean velocity is dropping once we go through the screens and for that reason the coefficient of variation of the velocity was also calculated. In both cases the screens smear out nearly all the non-uniformities of the velocity profile in the tunnel, reducing the measure of variation by about an order of magnitude.

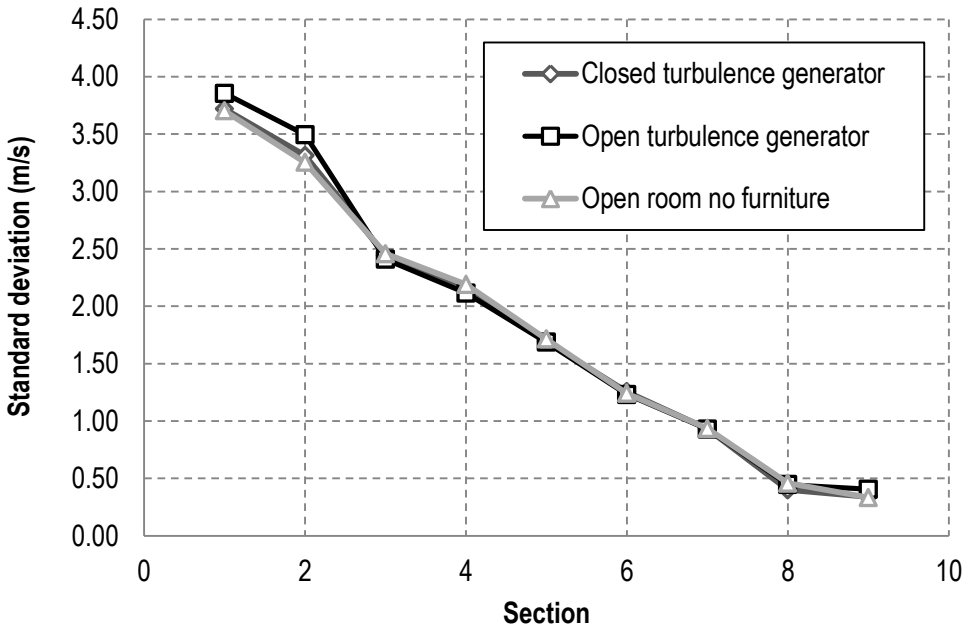

Figure 2.14: Area averaged standard deviation of the air velocity in the tunnel

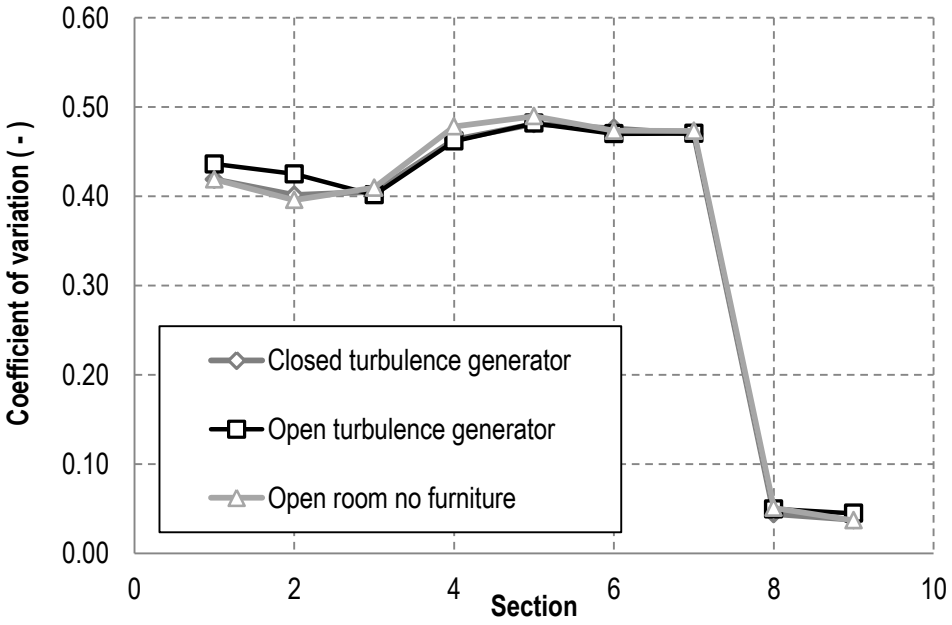

Figure 2.15: Area averaged coefficient of variation of the air velocity in the tunnel

Table 2.1 lists the mass flow rate calculated for the same three models. Again it can be noticed that despite the fact of considerable change in the model – translation of all the walls and removal of the turbulence generator, the amount of the air going through the inlets is not changing significantly.

Table 2.1: Mass flow rate through the fan inlets

Model	Left side	Right side
Closed turbulence generator	18.713 kg/s (15.54 m^3/s)	17.058 kg/s (14.17 m^3/s)
Open turbulence generator	19.250 kg/s (16.25 m^3/s)	16.630 kg/s (14.04 m^3/s)
Open room	18.870 kg/s (15.94 m^3/s)	16.700 kg/s (14.10 m^3/s)

To summarize, the flow through the tunnel appears to be insensitive to the changes in the room geometry that were tested up to this point in the modeling effort. Yet additional runs for the cases with fully furnished room need to be performed to check the magnitude of the effect of current room furniture on the air flow uniformity. Note that a more detailed and accurate model of the fan would also influence the results. However, the big picture is expected to remain largely unchanged with minor changes to the fan model geometry.

3. Refined Model of the Wind Tunnel Screens

A study of the TFHRC wind tunnel CFD modeling was initiated in the previous quarter. The CFD model of the wind tunnel was created based on the CAD data provided by TFHRC. Multiple runs of the air flow through the tunnel in the laboratory room were conducted. In the initial runs the lab furniture was not included in the models. Also the method of modeling the screens in the tunnel as porous baffles was simplified. In the current quarter the most representative simulations out of the ones without the furniture were repeated with enhanced modeling of the screens. Also the model with the furniture in the lab room was created and analyzed. The current report documents the enhancements and the new results.

To replicate the screens installed in the tunnel a model of porous baffles was used. According to the STAR-CCM+ user guide [1] the pressure drop across a porous baffle can be modeled with the following equation:

$$\Delta p = -\rho(\alpha|v_n| + \beta)v_n \qquad 3.1$$

Where:

ρ - is the density of air,

v_n - is the normal velocity of air acting on the screen and

α and β are parameters that depend on screen geometry and properties.

In the literature only information about the possible derivations of α were found and the equation 2.1 was usually simplified to a form [2]:

$$\Delta p = -\frac{1}{2}K\rho {v_n}^2 \qquad 3.2$$

In the initial runs β parameter was assumed to be zero and α parameter was assumed to be constant (α = 0.3632). Setting parameter β to zero in Equation 2.1 we could relate α to the K parameter as:

$$K = 2\alpha \tag{3.3}$$

A more advanced formula by Weighardt defines *K* as a function of air normal velocity on the screens [3]:

$$K = 6.5\left[\frac{1-\chi}{\chi^2}\right]\left[\frac{v_n d}{\chi v}\right]^{-\frac{1}{3}} \tag{3.4}$$

Where:

v_n - is the air velocity normal to the screens,

d - is the screen wire diameter and

ν - is the kinematic viscosity of the air.

Taking the diameter of the screen wire as 0.0075 inch, the kinematic viscosity of air as 15.68e-6 m/s^2 and normal velocity on the screens, the equation 2.5 was used to calculate α parameter each iteration using STAR-CCM+ field functions. The ideal definition would allow for taking into account a local value of the velocity on the screens. That would result in variable porous baffle parameters within a screen. However, this was not possible in the STAR-CCM+ and the velocity was taken as a surface averaged normal velocity of air. In Table 3.1 velocity measurements on the screens and calculated values of α for the model without the furniture are listed. The values for alpha are substantially different from the assumed initial value of 0.3632.

Table 3.1: Alpha parameter variation on the screens

screen number	normal velocity (m/s)	alpha (-)
1	8.532	0.442
2	8.498	0.442
3	6.516	0.483
4	4.937	0.530
5	3.803	0.578
6	2.892	0.634
7	2.118	0.703
8	1.847	0.736

3.1.1. Results

The first set of simulations model the system without the furniture in the room to determine the characteristics of the flow field in an empty room as a base case. In the initial model the mass flow through the fan inlet on the right side was 18.713 kg/s (15.54 m^3/s) and 17.058 kg/s (14.17 m^3/s) on the left side (The left side inlet is obstructed with a pulley plate for turning the fan). This reading was taken after 1000 iterations under steady state conditions. For each of the models additional 100 or more

iterations were requested at the end of the simulation with updated values of alpha for each of the screens. At this stage the mass flows were read again. At the side obstructed with the pulley (pulley-side) the mass flow changed to 18.078 kg/s (15.27 m^3/s) and on the other side (no-pulley-side) the mass flow changed to 16.765 kg/s (14.16 m^3/s). Overall the change was about 2.6 %. This value is very small and can be said that is in the range of the uncertainty as the mass flow is oscillating (in third digit) during the simulation and is not converging to a greater extent when the number of iterations in increased.

Table 3.2 shows comparison of the mean air velocities registered between the screens and on the inlet and outlet of the extension of the tunnel for both initial and updated model. There is a drop in the mean velocity because of the increased resistance of the porous baffles. However, the change is very small and for each section is less than 3.0 %. This tendency was registered for all the other analyzed cases, so this comparison was not repeated in this report and only the final results are presented.

Table 3.2: Mean air velocity in the tunnel

location	initial model	updated model
section between 1st and 2nd screen	8.87	8.65
2 - 3	8.25	8.05
3 - 4	6.03	5.87
4 - 5	4.60	4.48
5 - 6	3.52	3.43
6 - 7	2.63	2.56
7 - 8	1.99	1.94
extension in	9.04	8.80
extension out	9.04	8.80

The model with the furniture was also updated. The cabinet was rotated and placed next to the tunnel's wall, as it is in the real lab. Figure 3.1 and Figure 3.2 show the velocity distribution in the lab in two cross sections – vertical and horizontal respectively. The horizontal cross section was created above the level of the computer desks so they are not visible in the figure. The higher elements of the furnishing are not influencing the returning flow to the fan inlets. 16.827 kg/s (14.21 m^3/s) of air is flowing through the obstructed fan inlet. 17.894 kg/s (15.11 m^3/s) of air is flowing through the other side of the fan. This is very close to the amount of air flowing through the fan in the model without the furniture in the room. The furniture is not negatively influencing the air mass flow in the lab.

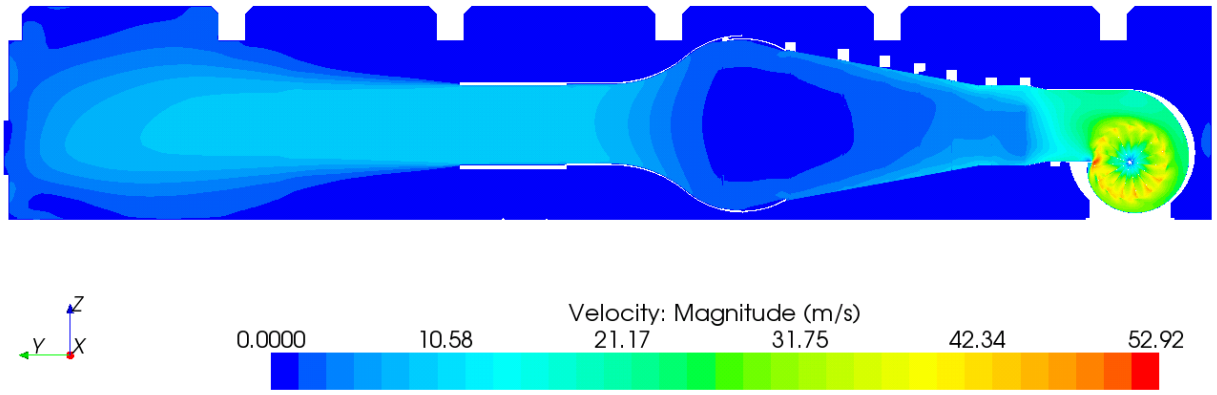

Figure 3.1: Velocity profile in model with the furniture – vertical plane

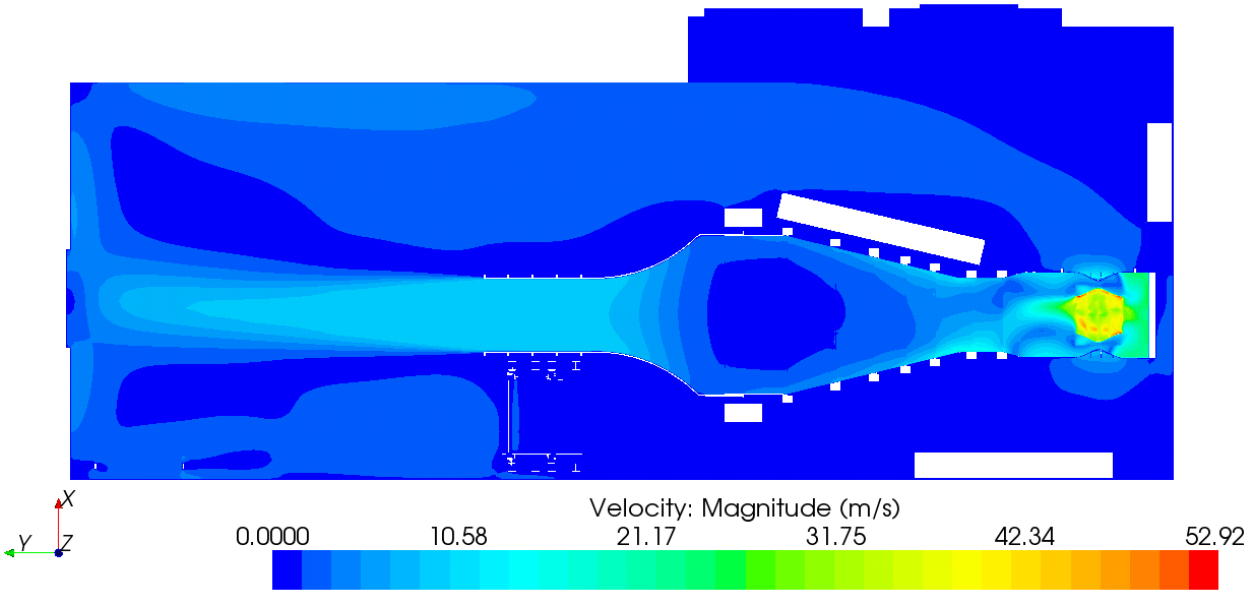

Figure 3.2: Velocity profile in model with the furniture– horizontal plane

Table 3.3 shows the surface averaged velocity of the air on the screens and corresponding to it the value of the alpha parameter. The values are not much different from the values in Table 3.1 for the model without the furniture.

TFHRC was interested in the quality of the flow inside of the tunnel extension and outside of it, approximately 4 to 5 ft downstream of the exit where tested objects are installed. For that purpose additional derived parts were created as vertical squares with the cross section size of the wind tunnel extension. In this report main focus was on the velocity distributions in the test sections, which are not in an enclosure, but out in the room.

Table 3.3: Alpha parameter variation on the screens

screen number	normal velocity (m/s)	alpha (-)
1	8.493	0.442
2	8.449	0.443
3	6.486	0.483
4	4.913	0.531
5	3.781	0.580
6	2.876	0.635
7	2.107	0.704
8	1.865	0.733

The following sections were considered:

- Outlet of the tunnel extension
- 2 ft beyond the outlet
- 3 ft beyond the outlet
- 4 ft beyond the outlet
- 5 ft beyond the outlet
- 6 ft beyond the outlet

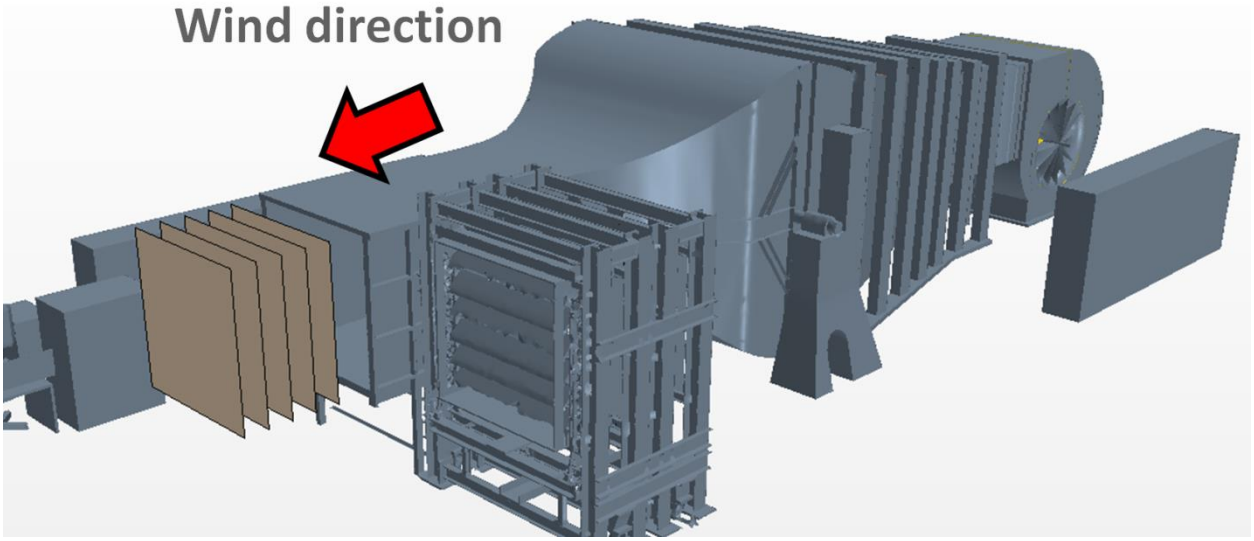

Figure 3.3: Location of the sections of interest in the model

When initial models and meshes were built and tested, the test section was assumed to be in the tunnel extension and a fine mesh in the internal flow region was judged to be sufficient. The mesh has now gone through several refinement tests for about 2 hydraulic diameters downstream of the tunnel exit for better assesment of the flow quality outside of the tunnel. As previously noted the room geometry and end wall have very little effect on the internal flow past the first couple of screens, but in an

external test zone, there are some room effects. The computational mesh around the testing section was significantly refined (cell size on the edges ~ 0.9 in). Figure 3.4 shows the new mesh outside of the tunnel extension in the testing section. The geometry of the pulley was not updated yet and it is still represented as a solid disc as it was in the CAD files. A recent meeting at the test facility revealed that the pulley is actually an open wheel with spokes, and that geometry will be incorporated into the model.

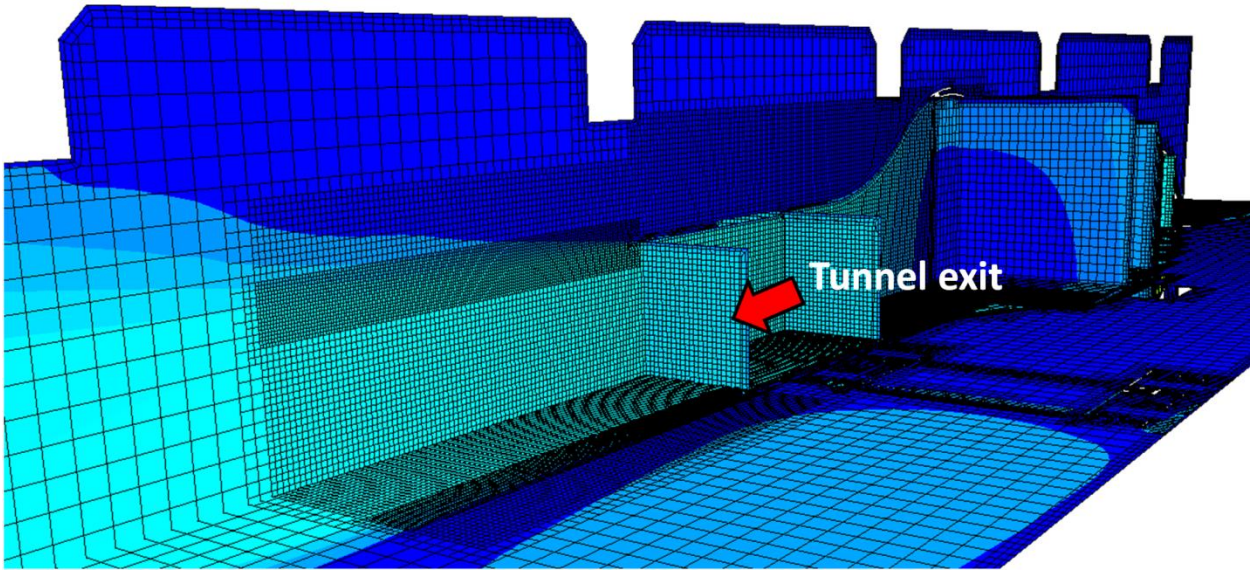

Figure 3.4: Mesh refinement outside of the tunnel extension

A literature search was performed on jet half angles. Based on G. Horn & M. W. Thring "Angle of Spread of Free Jets" Nature 178, 205 - 206 (28 July 1956) measured values of the jet half-angle have been variously reported from 7° to 20°. Using Prandtl's hypothesis, Tollmien calculated the jet half-angle to be 12°. An estimate based on our CFD analysis indicates that the angle is about 13.5° (influenced by the interaction with the end wall and where you draw the line for measurement). This value is in agreement with estimates from the literature.

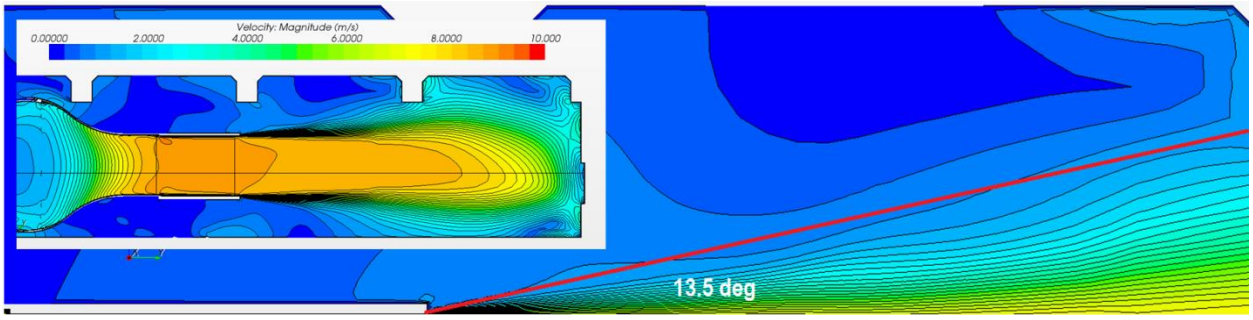

Figure 3.5: Measurement of the jet half-angle

The literature also indicates that the potential core (cone shaped for circular jets) will extend between 4 to 5 diameters downstream. The TFHRC test section is within one hydraulic diameter downstream of the tunnel exit, and the test bridges are close to the size of the exit opening width.

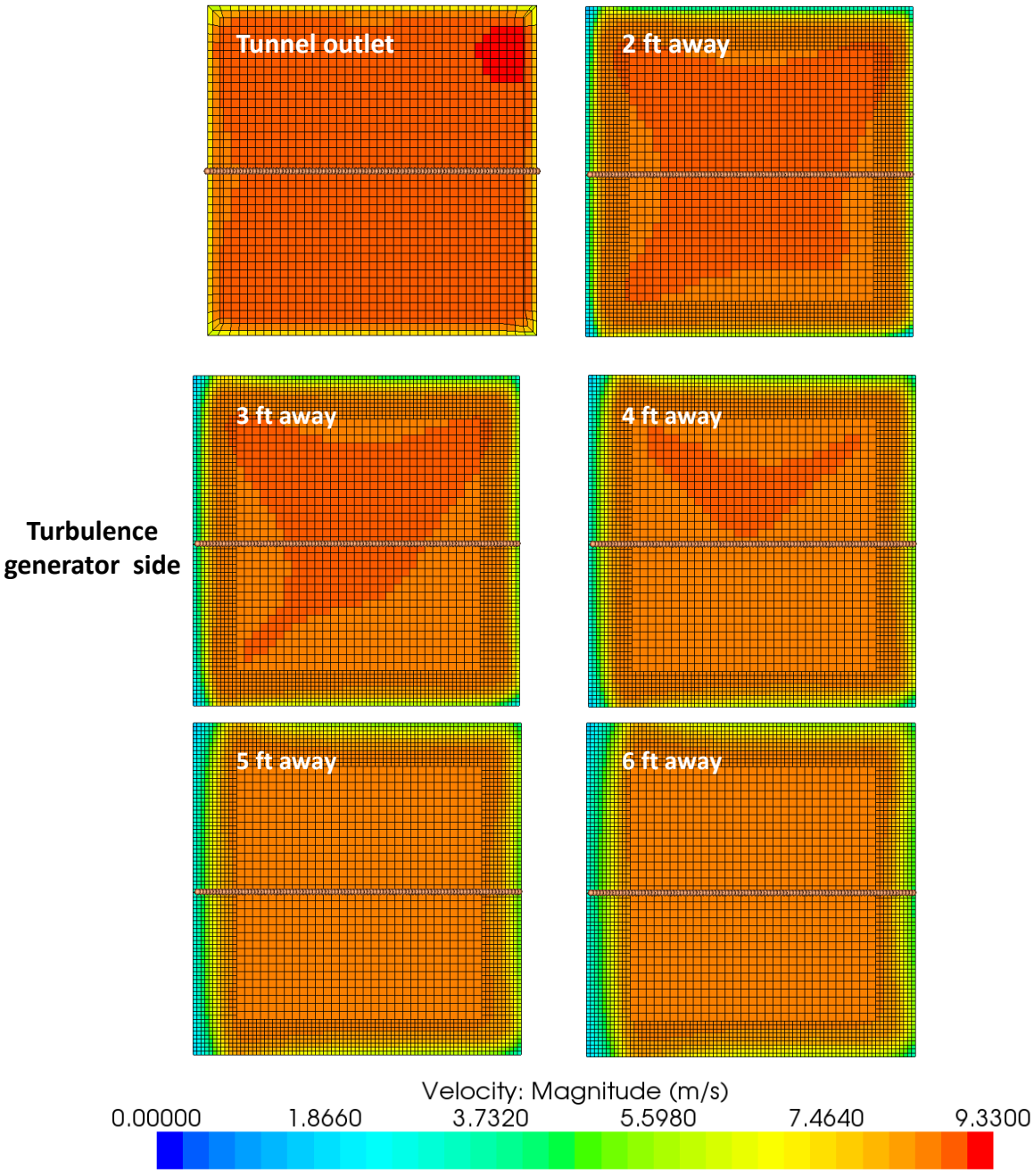

Figure 3.6: Velocity distribution in the section of interest

Figure 3.6 shows the velocity profiles in the testing sections. These profiles indicate that the velocity decreases more rapidly on the turbulence generator side of the jet than on the side with the larger amount of open space. Figure 3.8 present velocity distribution at the horizontal line running through the middle of the defined sections. The center of a 5 ft. bridge deck is shown aligned with the wind tunnel centerline. Asymmetries in room yield a smaller velocity drop on one side of the deck than the other. At 3 ft there is about 2 % drop in velocity at the ends. At 5 ft. downstream, a 8% drop on the turbulence generator side versus only a 4% velocity drop on the other side.

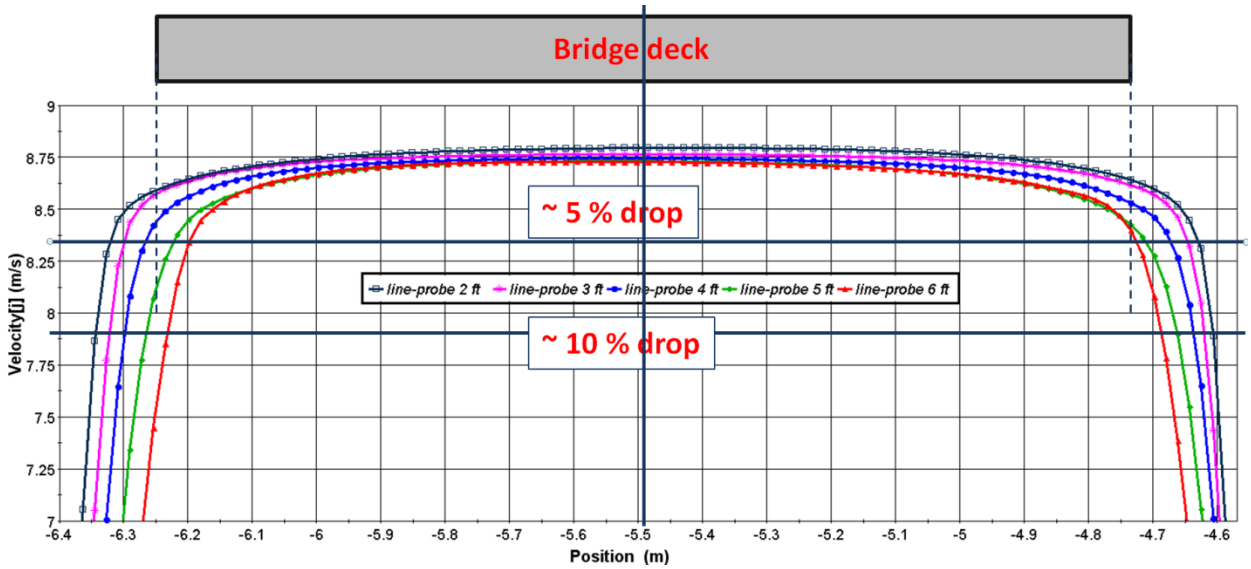

Figure 3.7: Velocity distribution downstream of the tunnel exit. Model with furniture, speed of fan 500 rpm.

Figure 3.8 presents a similar graph for the case where rotational velocity of the fan was dropped to 250 rpm from the initial value of 500 rpm. The velocity distribution in this case is more uniform on the edges of the bridge model. At 3 ft there is about 1 % drop in velocity at the ends. At 5 ft there is about 3 % drop on the turbulence generator side and about 1 % drop in velocity on the other side.

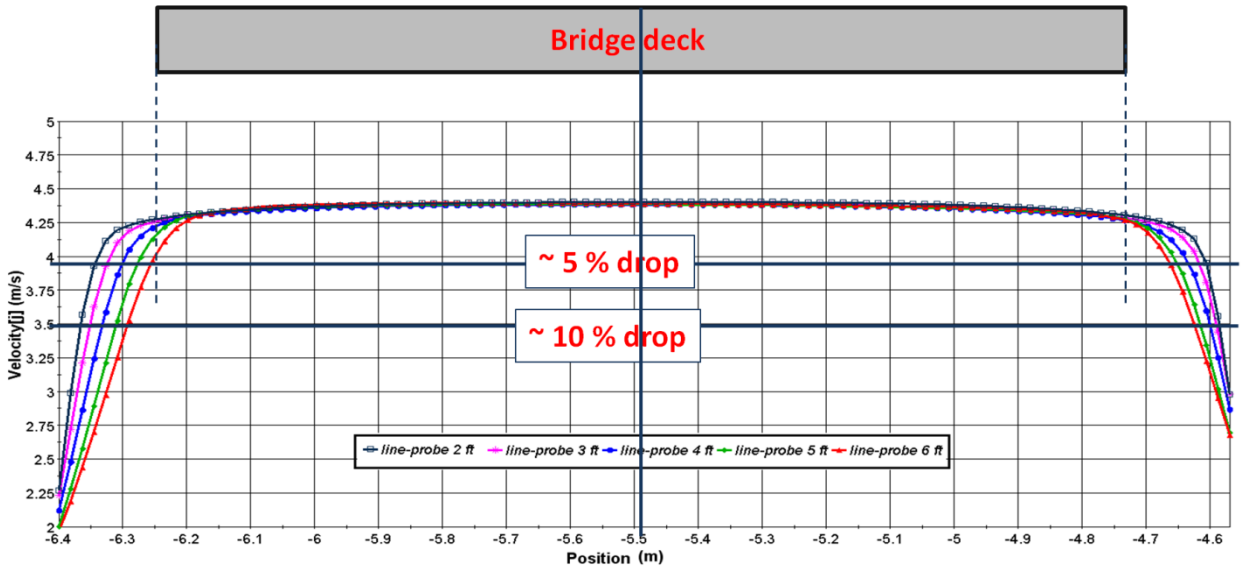

Figure 3.8: Velocity distribution downstream of the tunnel exit. Model with furniture speed of fan 250 rpm.

The model with the turbulence generator installed was analyzed. Figure 3.9 and Figure 3.10 show the velocity profiles in the room. Since the turbulence generator was not fully in its neutral position in the

provided CAD files, the flow is directed downward. The slight asymmetry in the jet observed without the generator also appears to be significantly amplified with the generator present.

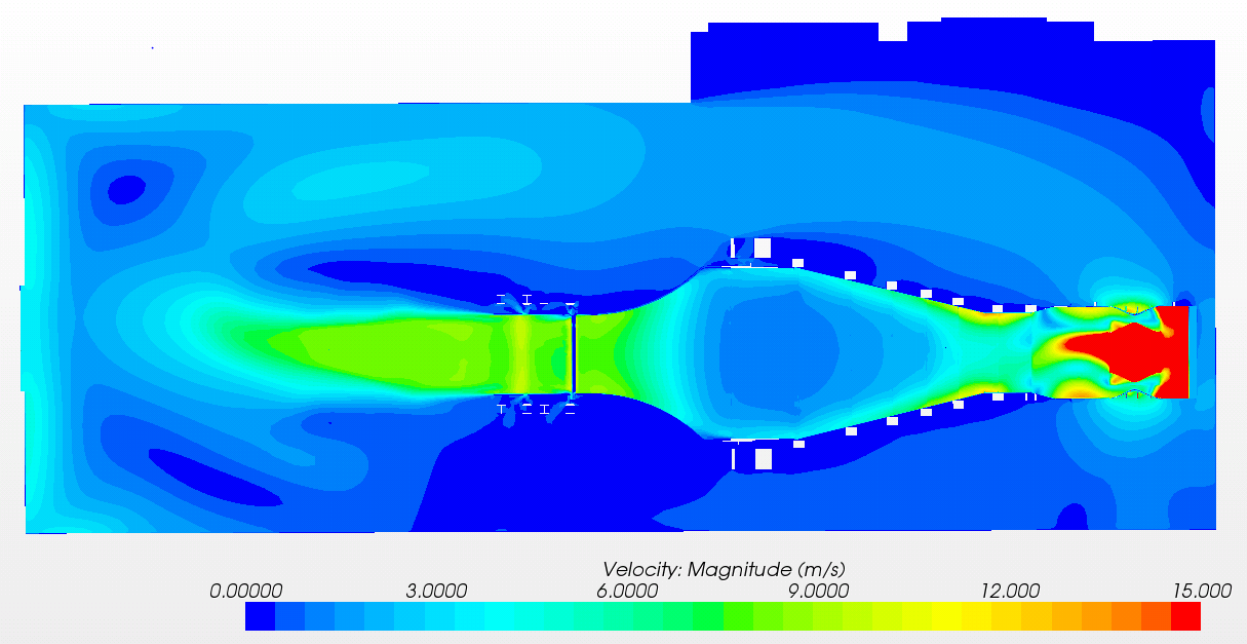

Figure 3.9: Velocity profile in model with the furniture – vertical plane

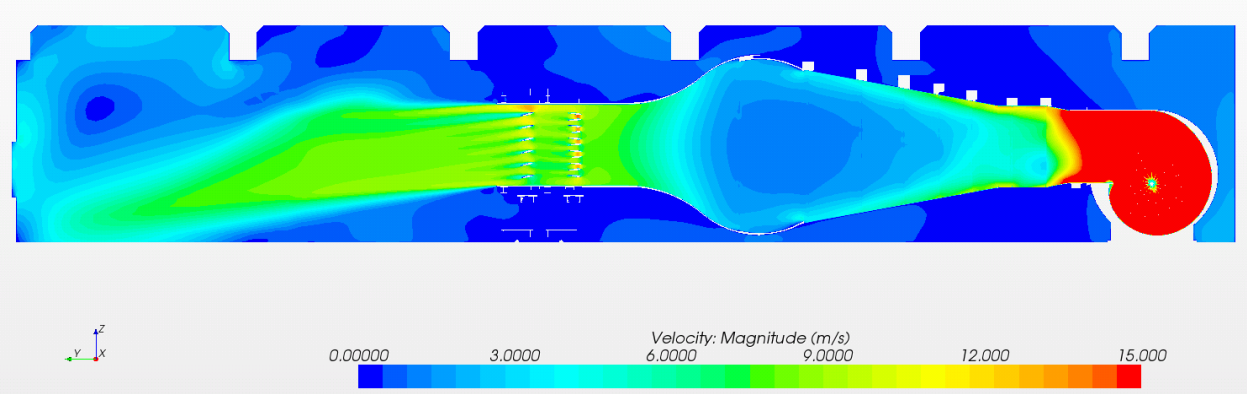

Figure 3.10: Velocity profile in model with the furniture – horizontal plane

Figure 3.11 shows velocity profiles in several cross sections outside of the tunnel. The further from the tunnel the more non uniform the flow is in the horizontal plane.

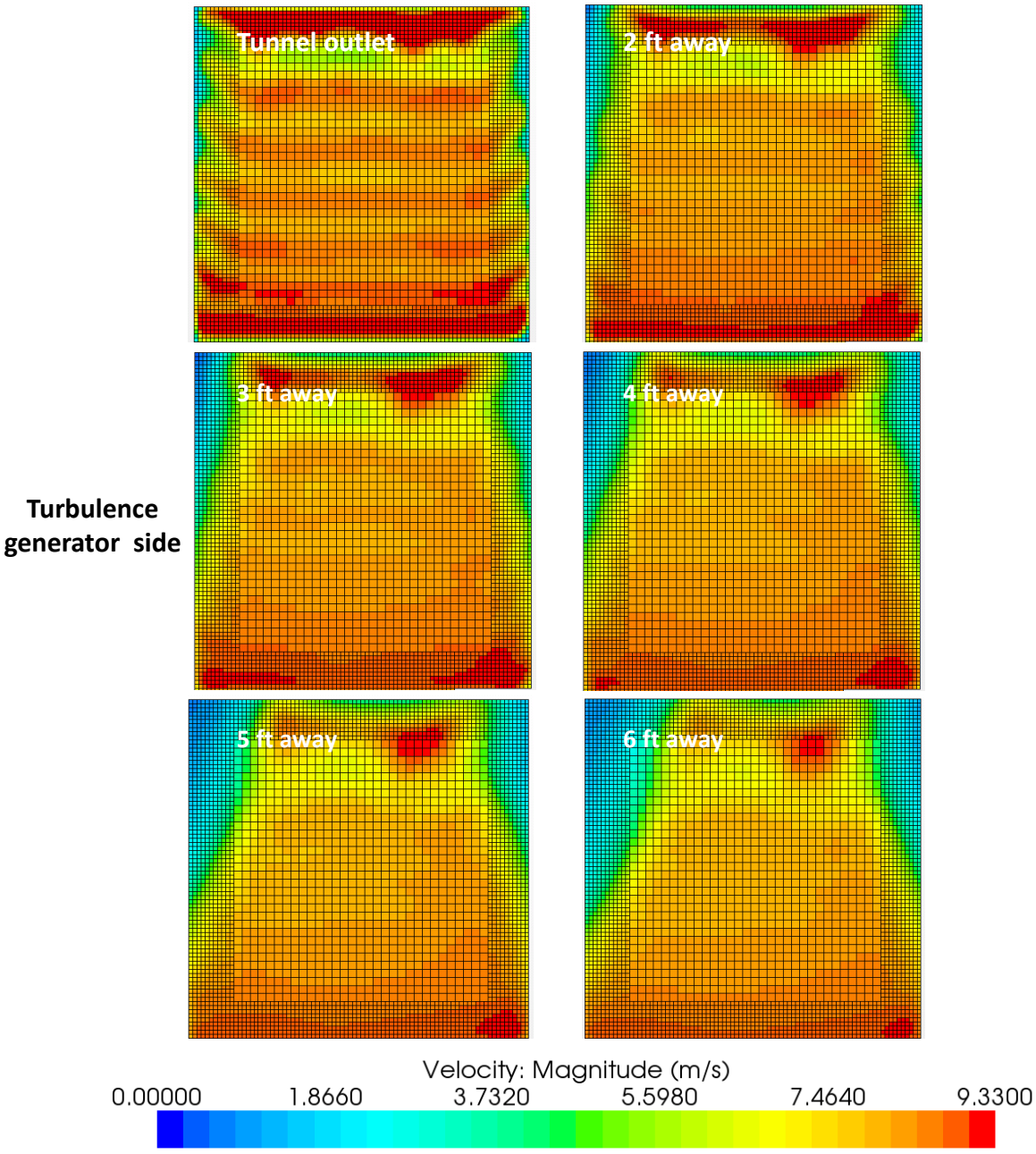

Figure 3.11: Velocity distribution in the section of interest

Figure 3.12 shows the velocity distribution at the horizontal line running through the middle of the defined sections with bridge deck aligned with the center of the wind tunnel. The plot shows a significant drop of the velocities on the edges of the testing section even for sections close to the outlet of the tunnel. Also the plot shows non-uniformity from left to right side of the room.

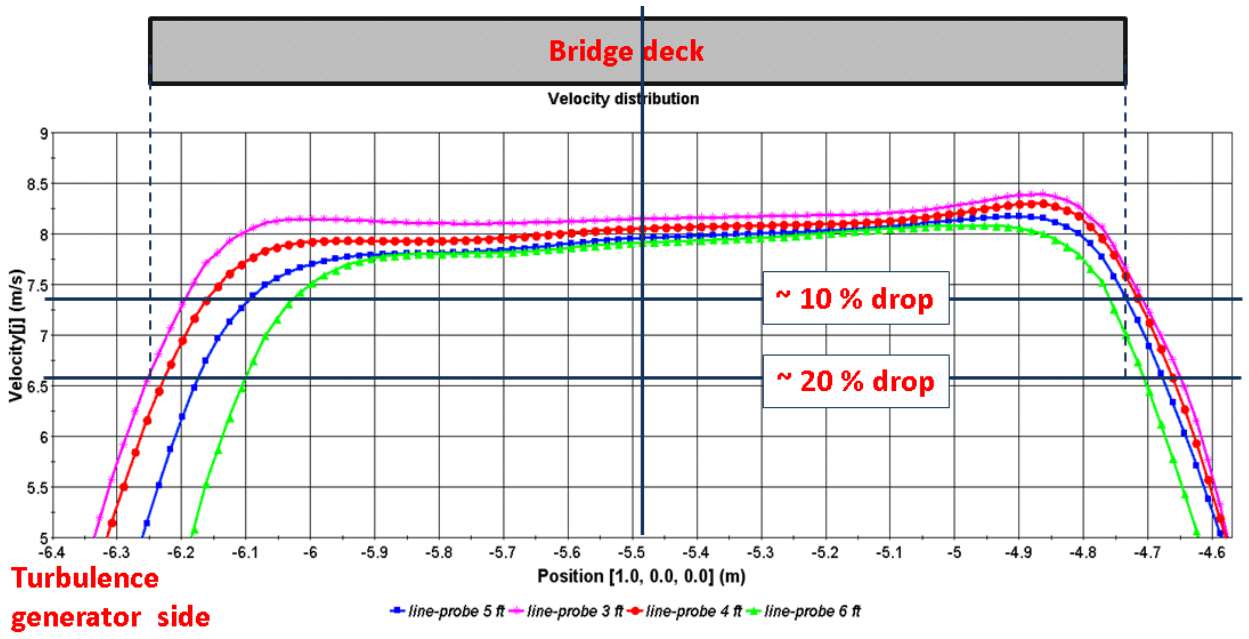

Figure 3.12: Velocity distribution downstream of the tunnel exit. Model with installed turbulence generator.

Further testing would be required to more fully determine the effects on the flow with the turbulence generator in the jet flow and to identify the probable causes of the flow pattern variations.

3.2. Modeling the Pulley with Spokes

The geometry files provided for the initial development of the wind tunnel and room model indicated the pulley on the fan drive shaft was a solid disk. A visit to TFHRC in January, 2012, included a tour of the wind tunnel laboratory, and during that visit, it was noted that the pulley was not a solid disk but was open with six spokes. The model was modified to have a pulley that matches the 6 spoke wheel of the laboratory, and the model was moved from version 6.04 to 7.02 of STAR-CCM+. The open spoke pulley on the side of the wind tunnel with the least resistance for return air flow was expected to increase the asymmetry in the test section in the simulations by a small amount.

An auxiliary model with reduced geometry to just the tunnel itself was built to study the effect of different models of the pulley on the mass flow rate through the tunnel. Specifically, it aimed at giving the answer to the question: how much air is let through the rotating pulley with the spokes. If the pulley is treated as a solid disk then this amount is equal to zero. On the other hand if it is not blocking the flow much while rotating, it might be treated as stationary to simplify the calculations. The geometry of the updated spokes and the simplified model are shown in Figure 3.13. The mass flow rate at the inlets was specified based on the previously completed simulations – the intake by the fan on both sides was measured. Several runs were performed to see the difference in mass flow through the pulley when using different rotation models:

- Stationary – the pulley with spokes is not rotating,

- Steady – the pulley with spokes is enclosed by a separate cylindrical region which is assigned a motion based on a moving reference frame. This motion model is preferable due to savings in the computation time when compared to the last case:
- Unsteady – the pulley motion is applied directly and the calculation is preformed using the implicit unsteady solver with a small timestep.

In each of the simulations the mass flow rate through the pulley (in the cross-section just behind the pulley) was tracked and compared. Figure 3.14 shows the flow through the simplified model with the rotating pulley model based on a moving reference frame.

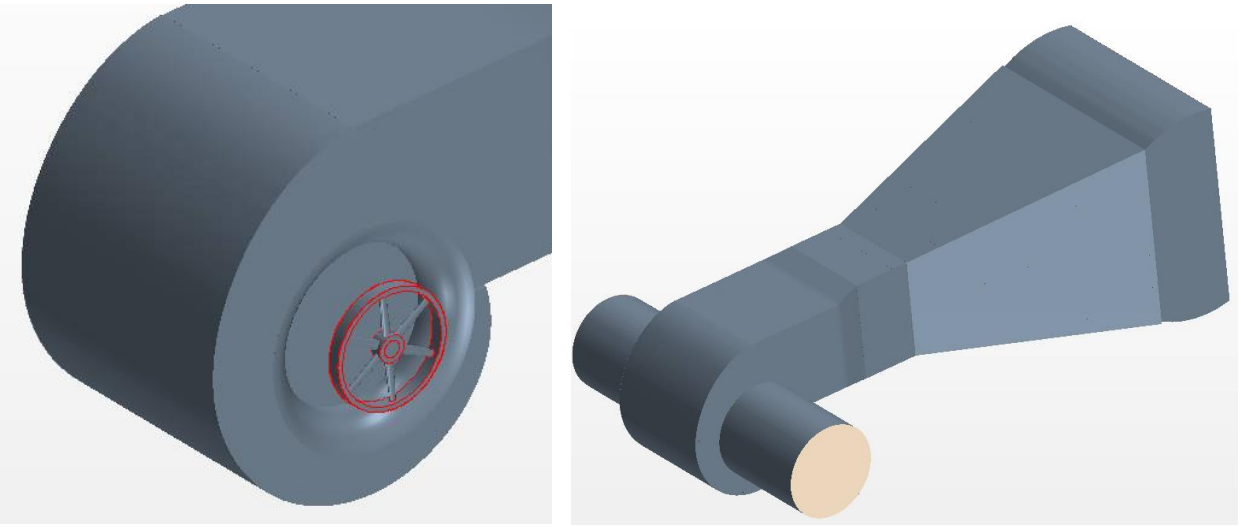

Figure 3.13: Auxiliary model to study the mass flow rate through the rotating pulley

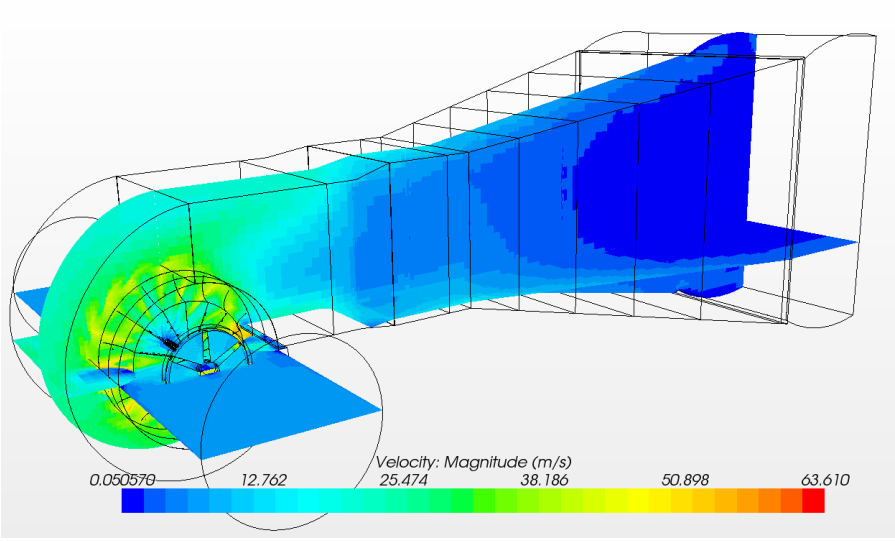

Figure 3.14: Flow through the simplified model with the rotating pulley based on the moving reference frame

Based on the test cases, it appears that modeling the pulley with direct rotation may not be feasible for modeling the whole laboratory room containing the wind tunnel. Decreasing the time step of the calculations helps to prevent divergence of the residuals in the model, but keeping the small time step

small for the overall simulation time of the flow in the entire room would make the computation time unreasonably long. Calculation with this model may be investigated further if needed to better quantify the effects of spokes in the pulley wheel. The unsteady (real rotation) was simulated until ~ 1 second of real time - two full rotations of the pulley. Work will be performed to run it for several more rotations.

Figure 3.15 shows the mass flow rate behind the pulley with spokes in two other models. They are very close in both cases.

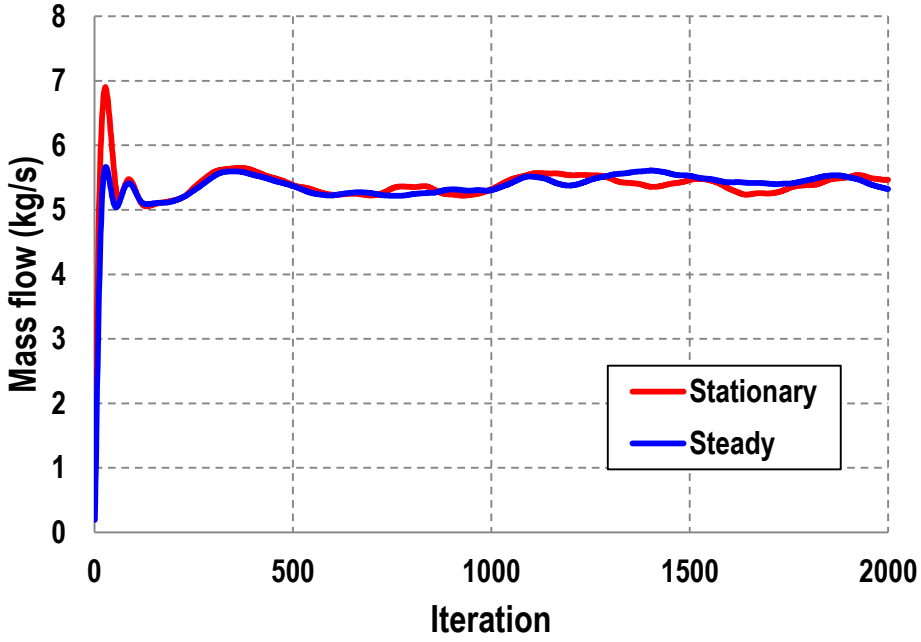

Figure 3.15: Mass flow rate through the pulley

The conclusions from these studies were as follows:

- It is hard to compute the detailed effects on the flow of the pulley with spokes.
- The simplified model of rotating turbo-machinery may not work well in this case because the pulley blades have no pitch and the pulley does not appear to act as a fan.
- To bound the possible solutions two extreme cases were analyzed:
  - Room with solid pulley - maximum blockage on the right hand side of the fan
  - Room without the pulley - no air flow blockage.
- The solution of the rotating pulley with spokes must lay between these two cases.
- If the difference between these two cases is not significant, either solution can be used as a valid one for the case of the rotating pulley with the spokes.

Figure 3.16 shows the velocity field in the room for the model without the spokes. There was no major difference noticed when comparing to the model with the pulley. Figure 3.17 shows a close up view of the testing sections located 2, 3, 4 and 5 ft behind the outlet of the tunnel with marked line probes. Figure 3.18 shows comparison of the velocities registered at these line probes. It can be noted that with this resolution of the plot the difference between the curves corresponding to the same location in the two models is barely noticeable. In close up view of the plot the asymmetry can be noticed on the

velocity distribution for the model without the pulley indicating the room effect. The difference however on both sides is below 1%.

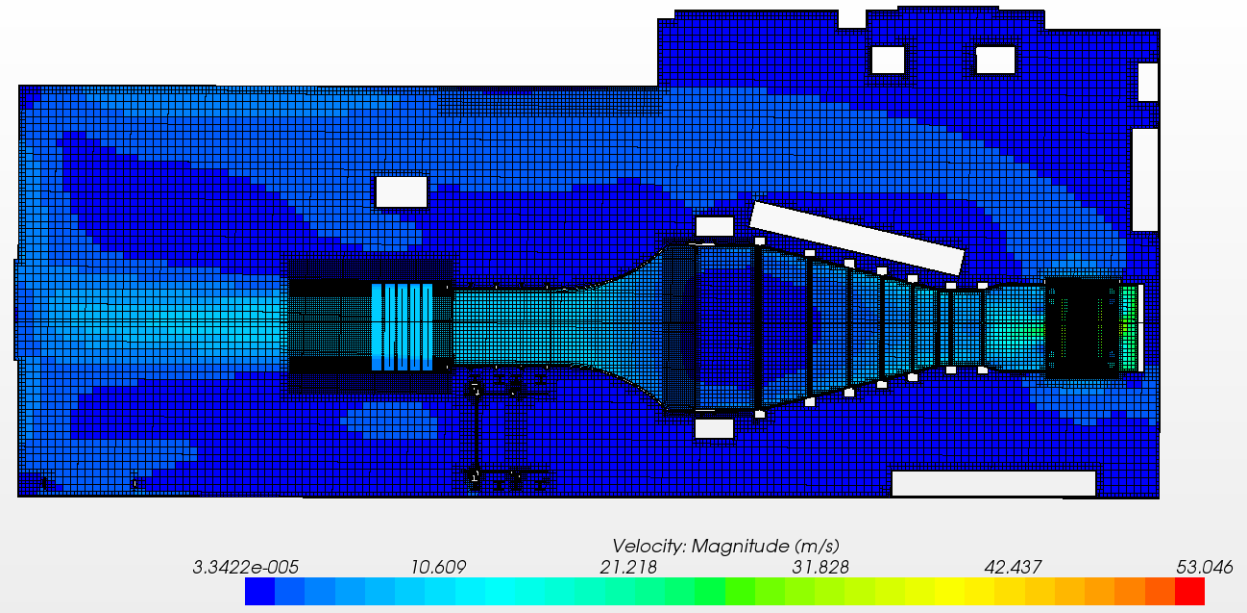

Figure 3.16: Velocity field in the model without the pulley

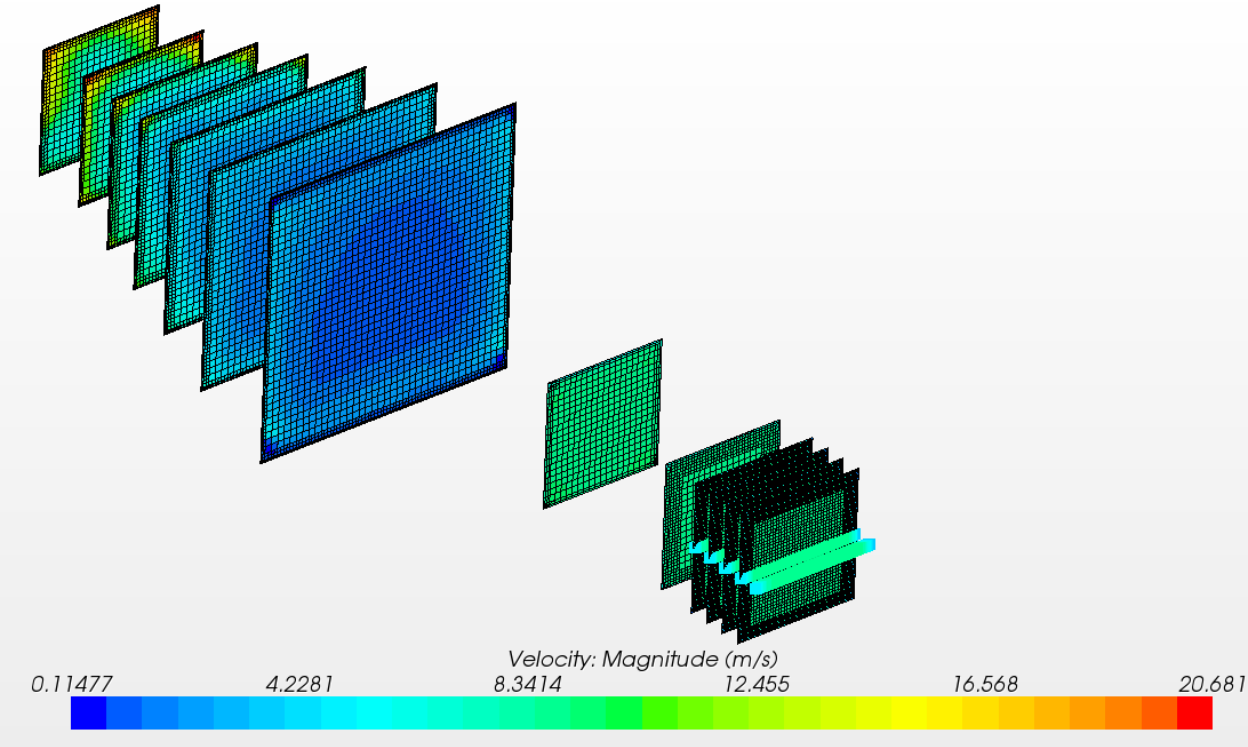

Figure 3.17: Close up view on the testing sections in the model

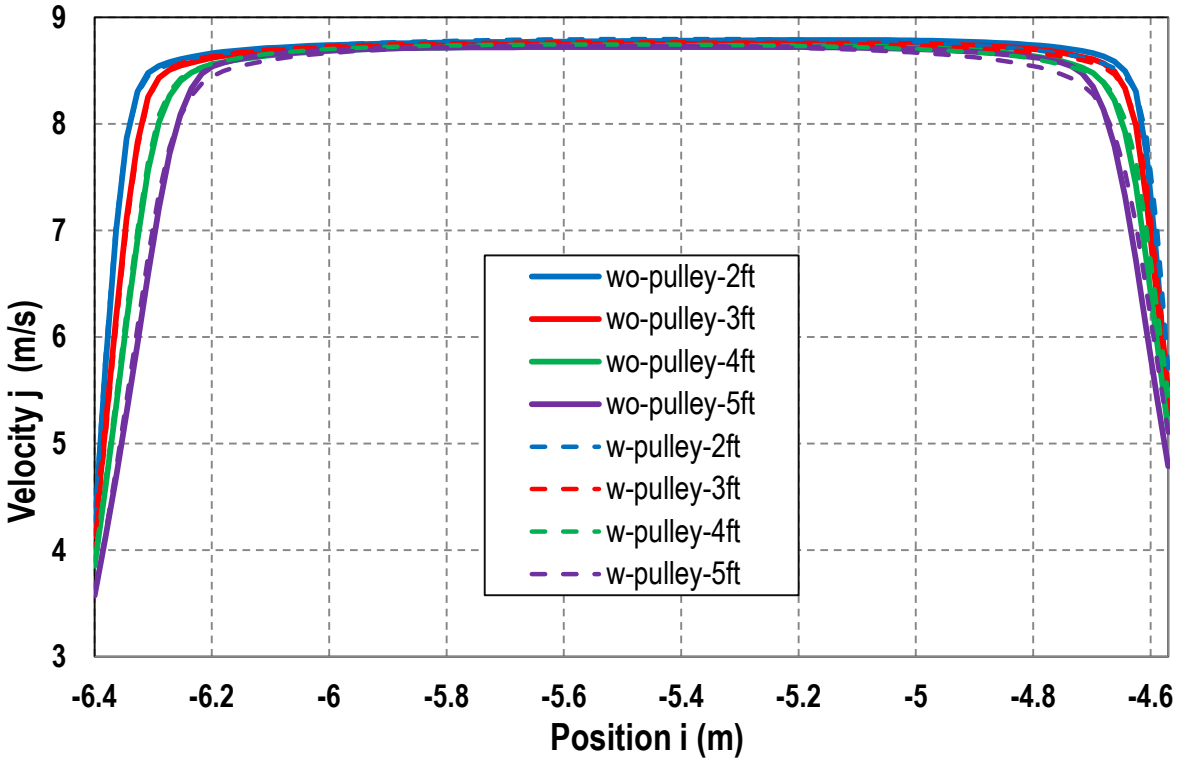

Figure 3.18: Comparison of the velocities at several locations in the test section for two models: with stationary disk pulley and no pulley at all.

4. Model Comparison with Laboratory Measurements

A comparison of laboratory air speed measurements with CFD calculated values was done to provide a means to calibrate the fan exit flow speed model and verify that flow predictions in the test zone at the outlet of the wind tunnel are adequately accurate. The fan model cage and blade geometry did not match that of the fan in the laboratory. The fan is old, although functioning very well, and details of the interior design of the fan blades and geometry are not readily available to construct an accurate, detailed CAD model of the fan, and the expense of doing it may not be justified. With the fan model running in a rotating reference frame, assigning a rotational speed equal to that of the laboratory test was found to under predict velocities at the wind tunnel exit by more than a factor of two. Most of the discrepancy is likely due to the inaccurate representation of the fan geometry, but some may also be due to the use of the rotating reference frame without the large computational additional expense of using a moving mesh. Because the primary zone of interest is at the exit of the wind tunnel, where test models are placed, an accurate fan geometry model may not be required at all. The interior of the tunnel, with screens between sections, is designed to produce a uniform flow at the outlet, even if the flow at the inlet, coming off the fan is significantly non-uniform. The test described in this section replaces the fan model with a velocity inlet that can be calibrated for a variety of fan rotational speeds. A uniform inlet velocity was then adjusted to match one measured point for the 118 RPM fan case, and results were compared to air speeds measured at 2.13 m (7 ft) above the floor.

4.1. Replacement of Fan Model with Specified Velocity Inlet and Pressure Outlets

Figure 4.1 shows the zones in the fan section of the wind tunnel, consisting of the fan, a swirl zone where air comes off of the fan blades and flows toward the entry chamber of the wind tunnel, and the entry chamber of the wind tunnel. This entire zone was isolated from the model by creating flat boundaries at the inlets and exit of the fan chamber to separate it from the room and the interior of the wind tunnel. The flow model is now the interior of the wind tunnel and the surrounding room, with the fan chamber excluded from the model. The inlet to the flow model in the rectangular inlet to the wind tunnel inlet chamber as shown in Figure 4.2, highlighted in pink. It is defined as a specified velocity inlet. The exits of the flow model are flat circular boundaries positioned at the narrowest part of the contracting fan chamber wall leading from the room into the fan as shown in Figure 4.3 highlighted in pink for the fan inlet on the far side of the room. These room exit boundaries are defined as pressure boundaries so that the flow split ratio on the two sides can be solved for as part of the model computation.

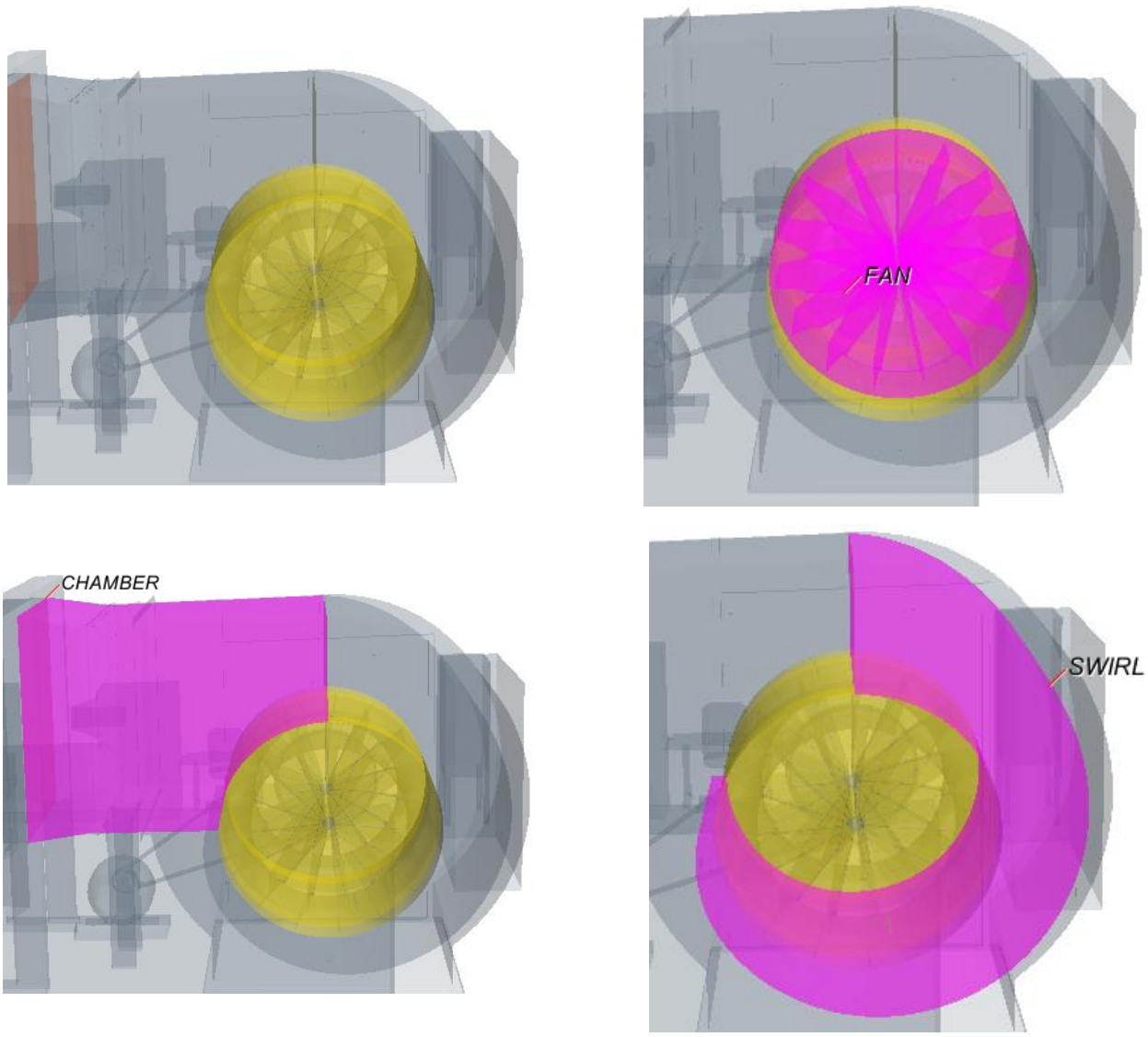

Figure 4.1 Zones in the fan section of the wind tunnel

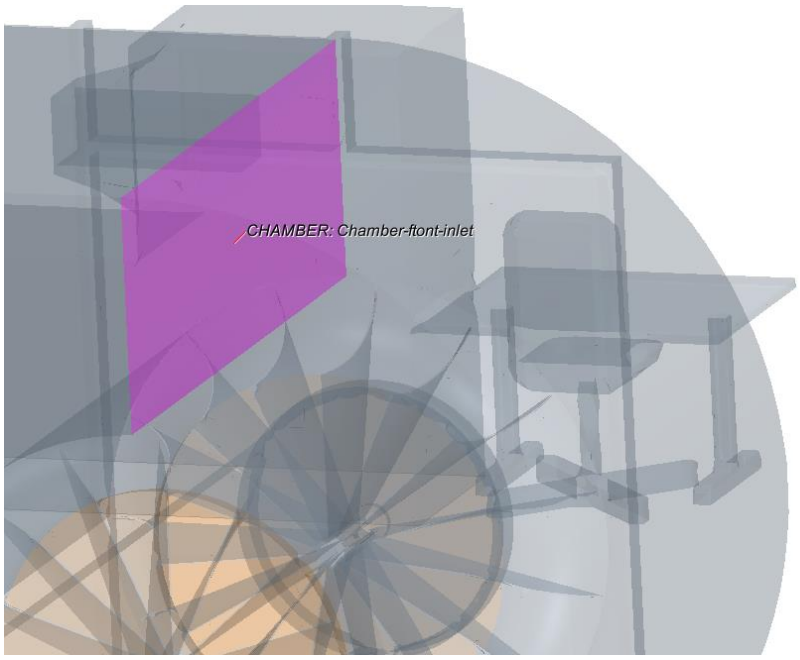

Figure 4.2 Portion of fan chamber showing inlet to wind tunnel in pink highlight

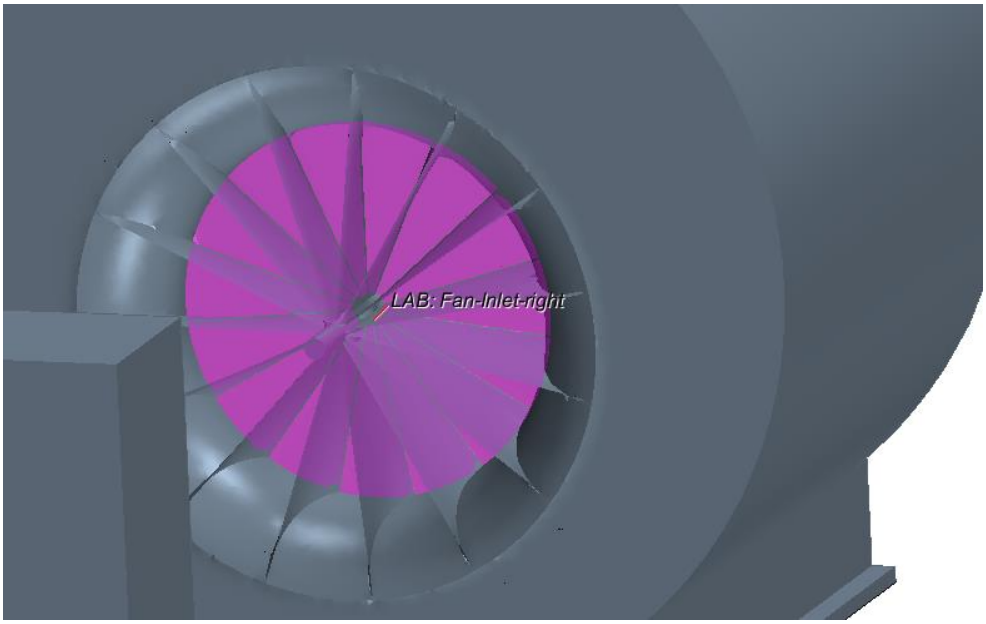

Figure 4.3 Portion of fan zone showing boundary between room and fan section in pink highlight

4.2. Determination of Inlet Velocity for Chamber Section

The volume flow through the rectangular wind tunnel entry shown in Figure 4.2 is not known for a given fan rotation speed. For this analysis the velocity across this inlet is assumed to be uniform, and it was iteratively adjusted until the velocity at laboratory measurement point 20, shown in Figure 4.6. This matching procedure is one way to use the CFD computation to calibrate the volume flow generated by the fan with the rotation speed of the fan. For the case with the motor running at 400 RPM and fan at 118 RPM, the velocity at measurement location 20 was 10.5 m/s (23.5 mph), and the average tunnel inlet boundary velocity required to match it was 21 m/s (47 mph).

4.3. Comparison of Laboratory Measurements and CFD Results

The computed velocity vector field at the laboratory measurement height is shown in Figure 4.4. The velocity vector field plotted from the laboratory measurements is shown in Figure 4.5. Vector lengths are proportional to velocity, however, they are scaled differently in the two figures to better show the flow pattern. The CFD results yield much more detail than the laboratory measurements. Note however, that the laboratory measurements at 2.1 m elevation included over 60 measurement locations in the room. As seen in the figures, the qualitative features of the flow field match reasonably well. The jet leaving the wind tunnel turns slightly to the right, as viewed from the fan end of the room, in both cases the CFD results and the measured values. Recirculation zones in the downstream end of the room are visible in both figures.

For a more quantitative comparison, computed and measured air velocities are compared across the wind tunnel jet downstream of the wind tunnel exit in Figure 4.7 to Figure 4.9. The CFD analysis predicts a slight asymmetry in the velocity distribution across the jet, as noted in previous sections. The measured values compare well to the computed values in the asymmetric distribution after matching of the velocity magnitude at point 20 via adjustment of the inlet velocity as described in Section 4.2. While the pattern of the distribution is similar, the CFD analysis under predicts the velocity on the right side of the room in the last row of measurement points near the far wall, Figure 4.9. In this location the computation is sensitive to the position of the stagnation point on the far wall. The jet at the exit of the wind tunnel is clearly influenced by the presence and location of the room walls. The confinement of the end wall forces the jet to stagnate, turn, spread out along the end wall, and ultimately turn back along the side walls to provide the return flow to the wind tunnel fan. Whether or not the asymmetry in the jet flow is sufficient to adversely influence drag, lift, moment, etc. measurements on objects placed in the test section just downstream of the wind tunnel exit is not addressed in the scope of this study. The presence of this asymmetry has been confirmed with the laboratory measurements.

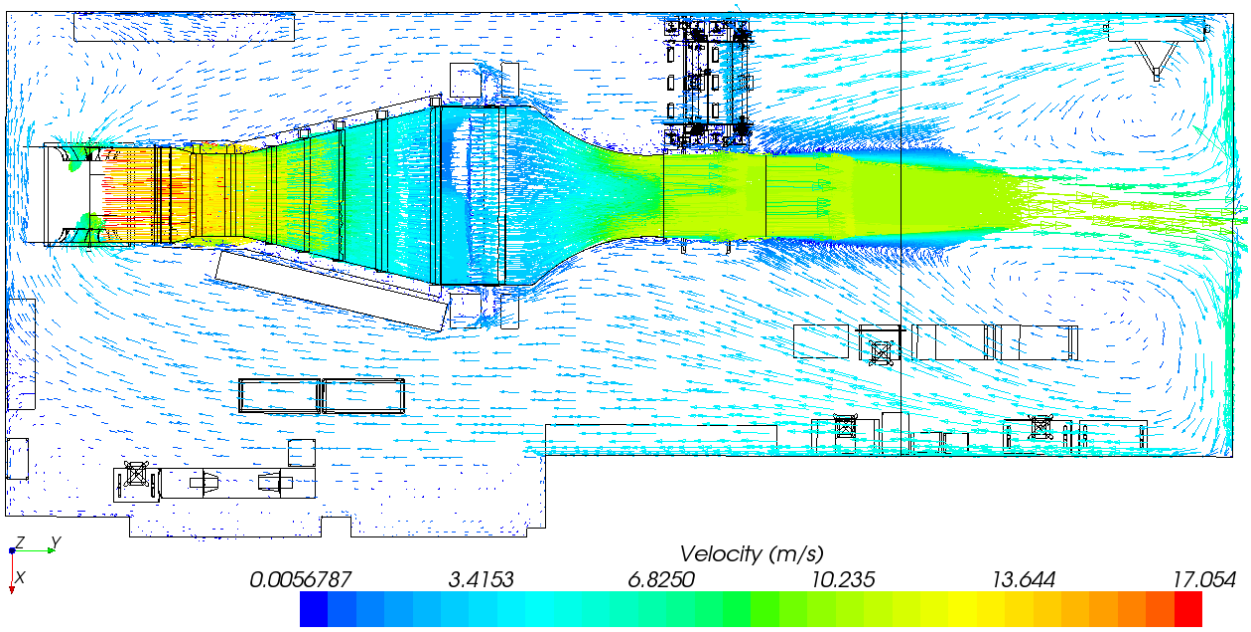

Figure 4.4 CFD computed velocity vector field at the height of the laboratory measurements

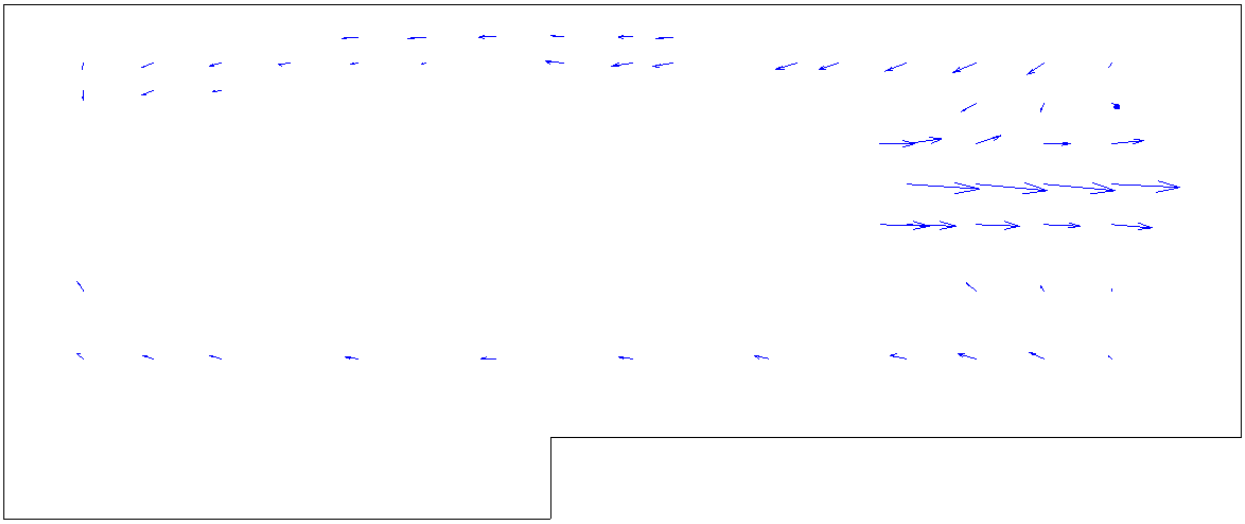

Figure 4.5 Vector field plotted from laboratory measurements

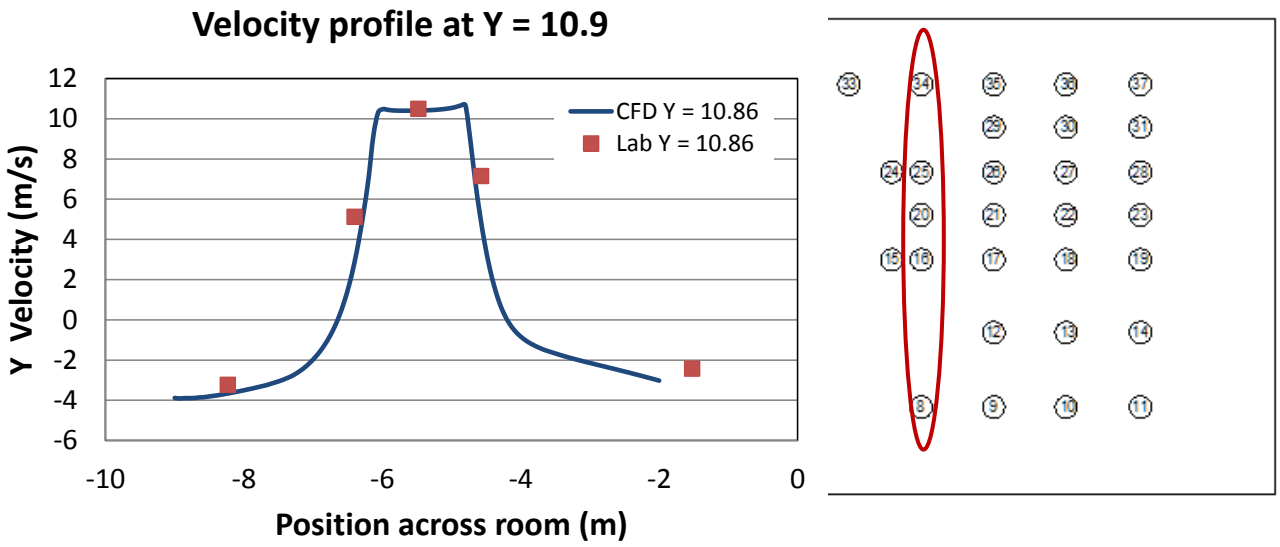

Figure 4.6 Comparison of measured and computed velocity distribution at first column of points that spanned the room. Point 20 was matched in the computation by adjusting the wind tunnel mean inlet velocity.

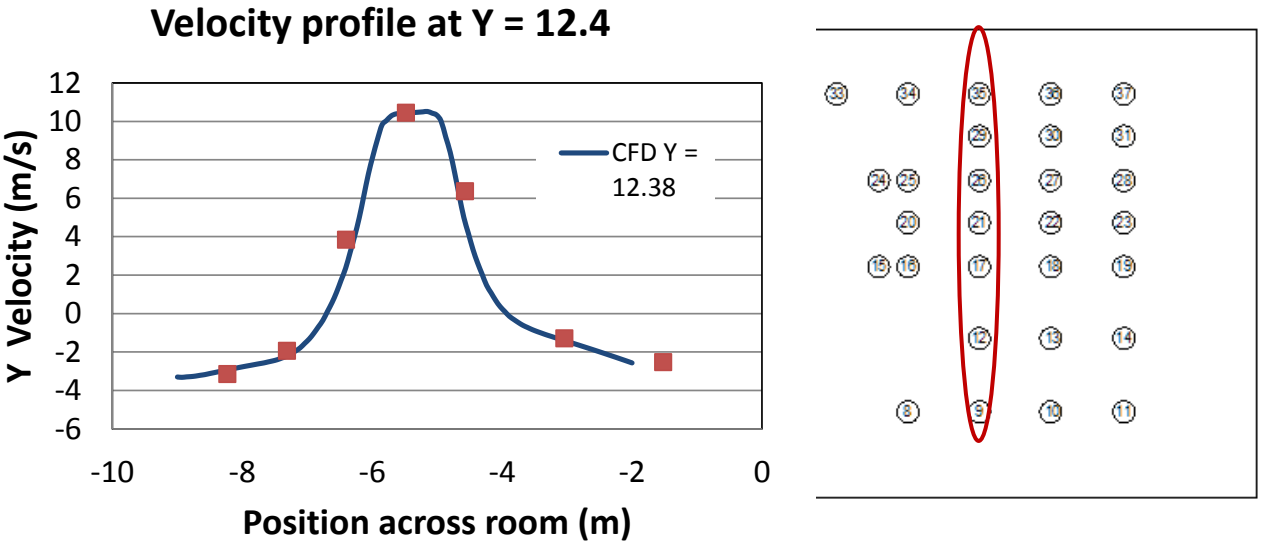

Figure 4.7 Comparison of measured and computed velocity distribution at the second set of measured points spanning the room in the downstream of the wind tunnel jet.

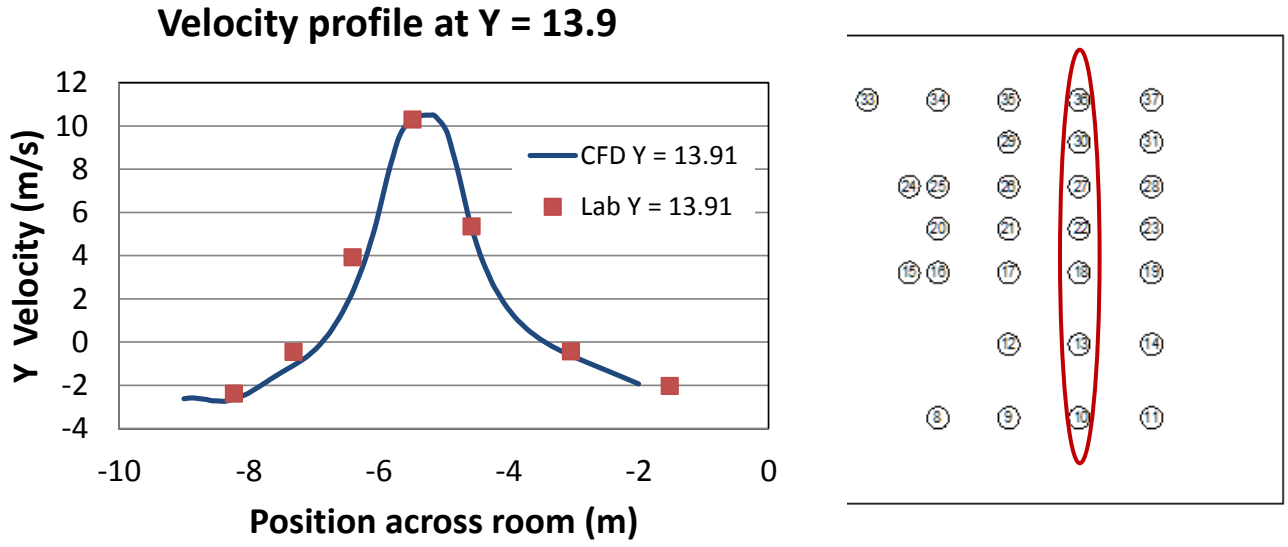

Figure 4.8 Comparison of measured and computed velocity distribution at the third set of measured points spanning the room in the downstream of the wind tunnel jet.

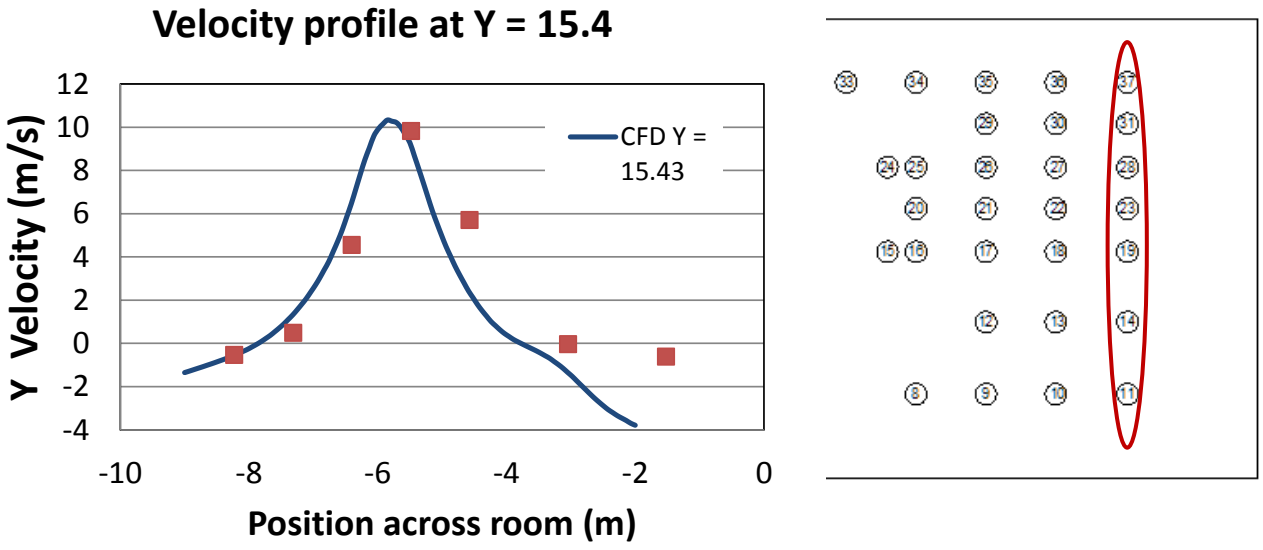

Figure 4.9 Comparison of measured and computed velocity distribution at the fourth set of measured points spanning the room in the downstream of the wind tunnel jet.

While the comparison between velocities computed with the CFD model and laboratory measurements at 2.1 m elevation in the main portion of the jet at the wind tunnel exit were quite good, the comparison along the return path to the fan near the walls is not nearly as good. The CFD computation uses a k-epsilon turbulence model, which is based on averaging the Navier-Stokes equations. However, the flow field computed in such a model does not necessarily correspond to average velocities over the entire domain of the room. Because the room in the model is a closed system, all of the air leaving the fan chamber should eventually re-enter the fan chamber through the two pressure exit boundaries on the sides of the fan chamber. In the computation, this condition, mass balance, is met very well. An air flow of 41.88 kg/s is propelled down the tunnel by the fan, and 41.88 kg/s enters the fan chamber from the room, 22.50 kg/s from the right and 19.38 kg/s from the left fan entry. That is a mass balance of four significant figures, which is quite good, for this type of computation in a complex geometry with nearly all of the furniture in the room represented in the model as well as the geometry of the tunnel, turbulence generator, etc. The eddy viscosity in the k-epsilon model determines the mean transport rate of momentum due to large fluctuating eddies in the room that are averaged out in the model. This includes the mixing with air surrounding the jet, which controls the entrainment rate and consequently, in part, the velocity distribution across the jet. These results compared well with lab measurements. The various obstructions in the room and the eddy viscosity contribute to determining the paths of least resistance for air to return to the fan. Since all air (to 4 digits) makes it back to the fan, over estimation of velocity at 2.1 m height near the right wall as shown in Figure 4.10, must be offset by under prediction at some other parts of the room. The velocities in Figure 4.10 show the correct trend, but the over prediction is fairly large between about the 6 m and the 11 m position. This region is not near the test section of the wind tunnel so error in this part of the domain does not have significant implications for testing the effects of wind on objects places in the wind tunnel jet.

Figure 4.11 shows a comparison of the measured and CFD computed mean velocity near the wall with the turbulence generator. The measurement points are shown circled in red. In this case the trend in velocity along the near wall return path to the fan is different at the measurement height between the measurements and the CFD calculations. The difference is approximately in the position of the turbulence generator, which represents a significant bluff body in the flow return path along the far wall, even though the vanes were open during measurement and in the model. The blockages of the sides of this object create a recirculation zone in the middle of the generator with a low velocity near the center of that zone. In reality, the sides of the generator may be shedding vortices that show up in measurement as significant velocity. The CFD turbulence model cannot capture vortex shedding accurately and the recirculation zone that results from the turbulence is steady and forces flow going back to the fan entry to bypass it. This situation appears to be the most likely cause of the measured and computed differences shown in Figure 4.11.

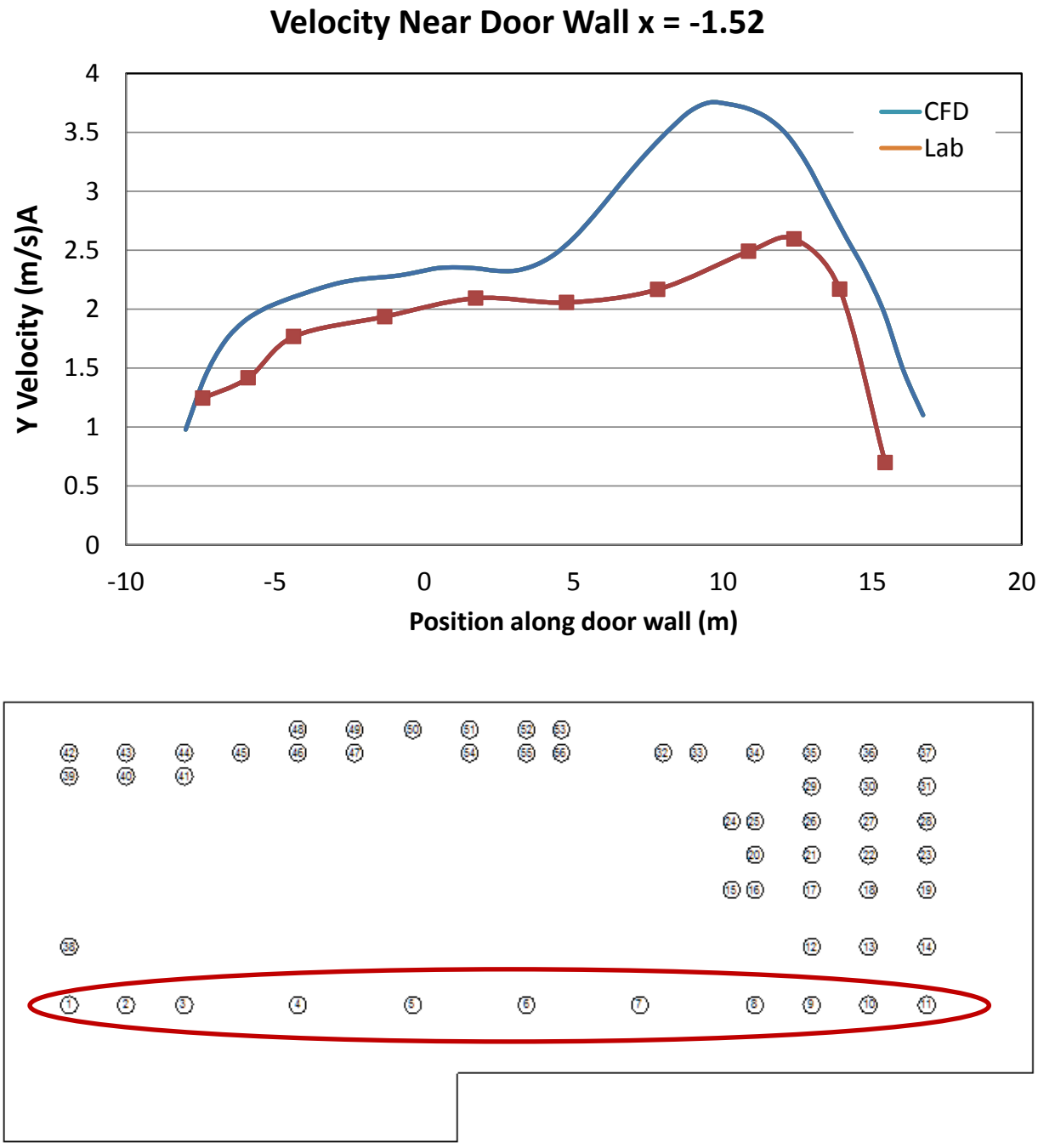

Figure 4.10 Measured and CFD velocity magnitude near the wall with the door (circled measurement points)

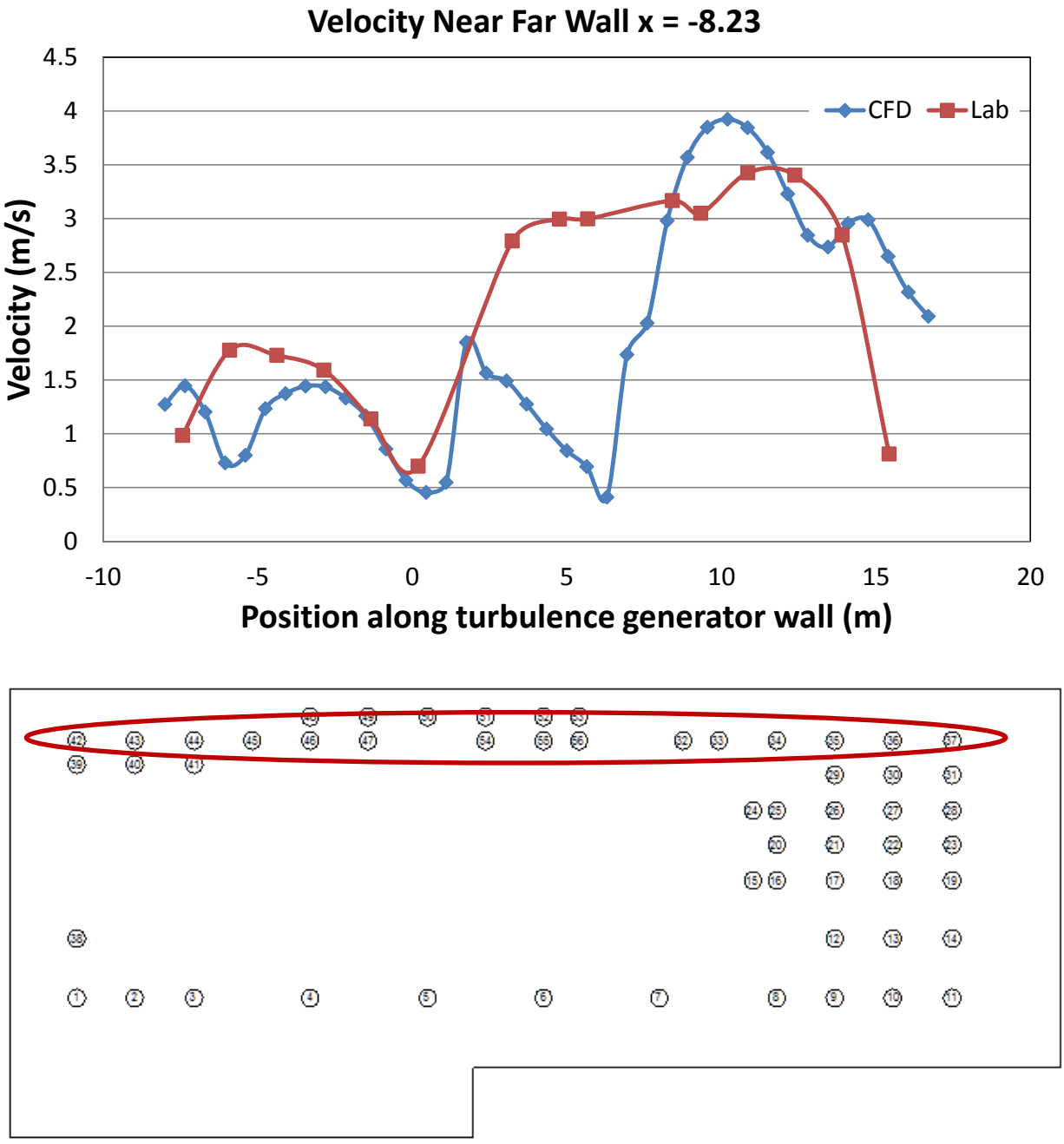

Figure 4.11 Measured and CFD velocity magnitude near the wall with the turbulence generator (circled measurement points)

5. Summary

A model of the wind tunnel laboratory at the Turner-Fairbank Highway Research Center was built including a very detailed geometry of the room, wind tunnel, and the furniture and other objects in the room. To provide for running the model on existing computer production high performance clusters with a one or two day turnaround time, a k-epsilon turbulence model was employed. Numerous reasonableness test were run with components of the model and submodels during their construction. These tests yielded physically realistic results. The model was also compared to one set of measured data in the laboratory at a measurement height of 2.1 m above the floor. CFD results in the wind tunnel jet matched well with the measured data. The jet is the region of most concern because test objects are suspended in this zone. CFD results along the walls did not compare as well to the experimental measurements. On the far side with the largest differences, they appear to be a consequence of the turbulence model and the obstruction of complex geometry of the turbulence generator. These areas of discrepancy were not in the zone of most importance, where objects would be placed for wind tunnel testing. The off center placement of the wind tunnel in the room does appear to slightly influence the symmetry of the air jet leaving the wind tunnel. The asymmetry appears to be a few percent at the edges of the jet, and was confirmed by air flow measurements. Shifting test objects slightly off the centerline may be one way to correct for the asymmetry if needed. The model is available for further testing and studies.

6. Acknowledgments

The funding for this project came from the 2005 SAFETEA-LU Transportation Bill under Title V, Section 5202C, capital improvement funds for the aerodynamics laboratory at the Turner-Fairbank Highway Research Center, through Interagency Agreement Number DTFH61-10-X-30040 between DOT and DOE, and the work was performed under DOE's contract with UChicago Argonne, LLC, Contract No. DE-AC02-06-CH11357. The authors would like to thank our FHWA sponsors, Harold Bosch, Research Structural Engineer and Aerodynamics Laboratory Manager and Kornel Kerenyi Hydraulics Research Program and Laboratory Manager at the FHWA Turner-Fairbank Highway Research Center for their support and many productive discussions on the modeling effort in collaborator videoconferences and meetings at both Argonne National Laboratory and the Turner-Fairbank Highway Research Center.

7. References

[1] McMaster-Carr, http://www.mcmaster.com/#wire-mesh/=emqkhc

[2] CD-adapco, *User Guide STAR-CCM+ Version 6.02.008*, 2011

[3] R.D. Mehta, *Turbulent Boundary Layer Perturbed by a Screen*, AIAA Journal, Vol. 2, No. 9, pp 1335-1342, September 1985

[4] R.D. Mehta, P. Bradshaw, *Design rules for small low speed wind tunnels*, The Aeronautical Journal of the Royal Aeronautical Society, November 1979

Energy Systems Division
Argonne National Laboratory
9700 South Cass Avenue, Bldg. 362
Argonne, IL 60439-4815

www.anl.gov